



Published in final edited form as:

Sci Immunol. 2017 January 27; 2(7): . doi:10.1126/sciimmunol.aal2200.

Potent and broad HIV-neutralizing antibodies in memory B cells and plasma

LaTonya D. Williams^{1,*}, Gilad Ofek^{2,*}, Sebastian Schätzle^{3,*}, Jonathan R. McDaniel^{3,*}, Xiaozhi Lu^{1,*}, Nathan I. Nicely¹, Liming Wu², Caleb S. Loughheed², Todd Bradley^{1,4}, Mark K. Louder⁵, Krisha McKee⁵, Robert T. Bailer⁵, Sijy O'Dell⁵, Ivelin S. Georgiev⁶, Michael S. Seaman⁷, Robert J. Parks¹, Dawn J. Marshall¹, Kara Anasti¹, Guang Yang¹, Xiaoyan Nie¹, Nancy L. Tumba^{8,9}, Kevin Wiehe^{1,4}, Kshitij Wagh¹⁰, Bette Korber¹⁰, Thomas B. Kepler¹¹, S. Munir Alam^{1,4,12}, Lynn Morris^{8,9}, Gift Kamanga¹³, Myron S. Cohen¹⁴, Mattia Bonsignori^{1,4}, Shi-Mao Xia¹, David C. Montefiori^{1,15}, Garnett Kelsoe^{1,16}, Feng Gao^{1,4}, John R. Mascola⁵, M. Anthony Moody^{1,16,17}, Kevin O. Saunders^{1,15}, Hua-Xin Liao^{1,4}, Georgia D. Tomaras^{1,15,16,18}, George Georgiou^{3,19,†}, and Barton F. Haynes^{1,4,16,†}

¹Duke Human Vaccine Institute, Duke University School of Medicine, Durham, NC 27710, USA

²Institute for Bioscience and Biotechnology Research, University of Maryland, Rockville, MD 20850, USA

³Department of Chemical Engineering, University of Texas at Austin, Austin, TX 78712, USA

⁴Department of Medicine, Duke University School of Medicine, Durham, NC 27710, USA

⁵Vaccine Research Center, National Institute of Allergy and Infectious Diseases, National Institutes of Health, Bethesda, MD 20814, USA

†Corresponding author. barton.haynes@dm.duke.edu (B.F.H.); gg@che.utexas.edu (G.G.).

*These authors contributed equally to this work.

SUPPLEMENTARY MATERIALS

immunology.sciencemag.org/cgi/content/full/2/7/eaal2200/DC1

Accession numbers

The accession numbers for the antibodies reported in this study for GenBank are KY272635 to KY272674. The accession numbers for the crystal structures reported in this study are 5U3J, 5U3K, 5U3L, 5U3M, 5U3N, 5U3O, and 5U3P.

Author contributions: L.D.W. produced antibodies, designed and performed experiments, analyzed data, and wrote and edited the manuscript. G.O. performed structural analyses and wrote and edited the manuscript. N.I.N., L.W., and C.S.L. also performed structural analyses. S.S., J.R.M., and G.G. performed analysis of plasma antibodies and high-throughput sequencing of paired V_H/V_L repertoire and wrote and edited the manuscript. X.L. isolated memory B cell antibodies. T.B. assisted with experimental design and edited the manuscript. M.K.L., K.M., R.T.B., S.O., J.R.M., M.S.S., D.C.M., S.-M.X., and M.B. performed neutralization assays. I.S.G., N.L.T., and L.M. performed neutralization plasma pattern analysis. R.J.P. performed autoantibody assays. M.A.M. and D.J.M. performed B cell sorting. K.A. and S.M.A. performed surface plasmon resonance and biolayer interferometry experiments. G.Y., X.N., and G. Kelsoe performed protein microarray analysis. K. Wagh and B.K. performed signature analysis and structural modeling. K. Wiehe, T.B.K., and F.G. designed experiments and performed sequence analysis. G. Kamanga and M.S.C. developed and managed the CHAVI cohort. K.O.S. and H.-X.L. produced antibodies. G.D.T. designed experiments. B.F.H. conceived and designed the study, analyzed data, performed autoantibody assays, and wrote and edited the manuscript.

Competing interests: B.F.H., L.D.W., M.A.M., X.L., G.O., H.-X.L., and K. Wiehe have filed patent applications on the DH511 lineage antibodies described in this study. The other authors declare that they have no competing interests.

Data and materials availability: Research materials used in this study are available from Duke University upon request and subsequent execution of an appropriate material transfer agreement. Coordinates and structure factors for the reported crystal structures have been deposited with the PDB under accession codes 5U3J, 5U3K, 5U3L, 5U3M, 5U3M, 5U3N, 5U3O, and 5U3P. Nucleotide and protein sequences for the heavy and light chain variable regions of the antibodies described in this study have been deposited within GenBank under accession numbers KY272635 to KY272674.

⁶Vanderbilt Vaccine Center and Department of Pathology, Microbiology, and Immunology, Vanderbilt University School of Medicine, Nashville, TN 37232, USA

⁷Beth Israel Deaconess Medical Center, Harvard Medical School, Boston, MA 02115, USA

⁸Centre for HIV and STIs, National Institute for Communicable Diseases, Johannesburg 2131, South Africa

⁹Centre for the AIDS Programme of Research in South Africa (CAPRISA), Nelson R. Mandela School of Medicine, University of KwaZulu-Natal, Congella 4013, South Africa

¹⁰Theoretical Biology and Biophysics, Los Alamos National Laboratory, Los Alamos, NM 87545, USA

¹¹Departments of Microbiology and Mathematics & Statistics, Boston University School of Medicine, Boston, MA 02118, USA

¹²Department of Pathology, Duke University School of Medicine, Durham, NC 27710, USA

¹³University of North Carolina Project-Malawi, Kamuzu Central Hospital, Lilongwe, Malawi

¹⁴Departments of Medicine, Epidemiology, and Microbiology and Immunology, University of North Carolina, Chapel Hill, NC 27599, USA

¹⁵Department of Surgery, Duke University School of Medicine, Durham, NC 27710, USA

¹⁶Department of Immunology, Duke University School of Medicine, Durham, NC 27710, USA

¹⁷Department of Pediatrics, Duke University School of Medicine, Durham, NC 27710, USA

¹⁸Department of Molecular Genetics and Microbiology, Duke University School of Medicine, Durham, NC 27710, USA

¹⁹Department of Molecular Biosciences, University of Texas at Austin, Austin, TX 78712, USA

Abstract

Induction of broadly neutralizing antibodies (bnAbs) is a goal of HIV-1 vaccine development. Antibody 10E8, reactive with the distal portion of the membrane-proximal external region (MPER) of HIV-1 gp41, is broadly neutralizing. However, the ontogeny of distal MPER antibodies and the relationship of memory B cell to plasma bnAbs are poorly understood. HIV-1-specific memory B cell flow sorting and proteomic identification of anti-MPER plasma antibodies from an HIV-1-infected individual were used to isolate broadly neutralizing distal MPER bnAbs of the same B cell clonal lineage. Structural analysis demonstrated that antibodies from memory B cells and plasma recognized the envelope gp41 bnAb epitope in a distinct orientation compared with other distal MPER bnAbs. The unmutated common ancestor of this distal MPER bnAb was autoreactive, suggesting lineage immune tolerance control. Construction of chimeric antibodies of memory B cell and plasma antibodies yielded a bnAb that potently neutralized most HIV-1 strains.

INTRODUCTION

Inducing broadly reactive neutralizing antibodies (bnAbs) is critical for developing a protective HIV-1 vaccine. bnAbs reactive with the envelope (Env) gp41 membrane-proximal

external region (MPER) have extensive neutralization breadth, and one of these, 10E8, reactive to the distal MPER, is one of the most broadly reactive HIV-1–neutralizing antibodies isolated to date (1–3). Two other MPER-binding gp41 bnAbs, 2F5 and 4E10, are both polyreactive, and their expression is limited by immune tolerance control in bnAb knock-in mice (4–7). In contrast, the 10E8 bnAb, in addition to potency and breadth, has lower reactivity with host molecules than 2F5 and 4E10 (1, 8–10). Thus, vaccine strategies for induction of 10E8-like antibodies are key to the development of an HIV-1 vaccine that can induce multiple broad and potent neutralizing antibody specificities.

Here, we have isolated a clonal lineage (DH511) of broad and potent Env gp41 distal MPER bnAbs from both memory B cells and plasma from an HIV-1–infected African individual, defined the DH511 developmental pathway, and demonstrated the reactivity of the DH511 unmutated common ancestor (UCA) with the A subunit of the autoantigen ribonucleoprotein (RNP), providing a mechanism of bnAb induction. Plasma DH511 bnAb lineage members were equally as potent neutralizers of HIV-1 as were bnAbs derived from memory B cells. Moreover, a chimeric DH511 lineage antibody consisting of memory bnAb V_H [variable region of immunoglobulin (Ig) heavy chain] and plasma bnAb V_L (variable region of Ig light chain) was broader than 10E8 and neutralized 99% of the HIV-1 isolates tested.

RESULTS

Isolation of memory B cell distal MPER gp41–neutralizing antibodies

Plasma of an African HIV-1 clade C chronically infected individual (CH0210) contained C-terminal (distal) MPER bnAb activity (11, 12). Six clonally related monoclonal antibodies (mAbs), designated DH511.1 to DH511.6 (named for antibody lineage “DH511,” with specific clonal lineage member “x” referred to as DH511.“x”), were isolated by antigen-specific single memory B cell sorting using MPER peptide fluorophore-labeled probes (Fig. 1, A and B, and table S1) (13). The DH511 B cell clonal lineage was distinguished by HCDR3 loops of 23 to 24 amino acids (table S1), and V_H and V_L somatic mutation rates were 15 to 22% and 14 to 18%, respectively. The DH511 clonal lineage was derived from the same heavy chain germline gene (V_H3–15) as the 10E8 gp41 bnAb but used a different V_L germline gene (DH511, V_κ1–39; 10E8, V_λ3–19) (table S1) (1). Antibody DH517, derived from a second clonal lineage arising from the same donor, was similarly isolated. DH517 used V_H4–34 and V_λ3–19 germline genes, was 22.8 and 14.3 % mutated, respectively, and had a long HCDR3 loop of 24 amino acids (table S1).

DH511.1 to DH511.6 and DH517 mAbs were assessed for neutralization breadth and potency against a panel of 30 HIV-1 isolates (table S2, A and B). DH511 clonal members neutralized each of the 30 isolates tested, with median 50% inhibitory concentrations (IC₅₀'s) ranging from 0.7 to 4.2 μg/ml (table S2A). DH517 had less breadth than DH511 clonal lineage antibodies, neutralizing 15 of 30 isolates with a median IC₅₀ of 5.7 μg/ml (table S2A). The most potent DH511 clonal lineage bnAb (DH511.2) neutralized 206 of 208 viruses (99%) in a panel of geographically and genetically diverse HIV-1 Env pseudoviruses and was slightly more broad but less potent than 10E8 (203 of 208, 98%) (median IC₅₀: 1.0 μg/ml for DH511.2 and 0.4 μg/ml for 10E8) (Fig. 1, C and D, and table S3). DH511.2 achieved >99% maximal neutralization for 93% of the isolates (Fig. 1E) and had similar

potency and breadth of neutralization against a second panel of 200 clade C primary HIV-1 isolates (table S4). Analysis of the Ig constant region sequences revealed that the naturally V_H/V_L -paired mAbs of both DH511 and DH517 clonal lineages were of the IgG3 isotype, as were 2F5, 4E10, and 10E8 (table S1) (1, 14, 15). These data raise the hypotheses that these MPER bnAbs either arose from a pool of precursor B cells that preferentially undergo class switching to IgG3 (16) or required IgG3 antibody flexible hinge region for optimal binding to HIV-1 virions or both.

Isolation of plasma

We next analyzed the MPER-specific plasma antibody repertoire from the HIV-1-infected individual CH0210 using an independent proteomics-based approach for the identification and semiquantitative determination of antigen-specific antibodies in human serum (17, 18). MPER-specific antibodies were isolated from a plasma sample by affinity chromatography, processed for bottom-up proteomics (19), and subjected to liquid chromatography high-resolution tandem mass spectrometry (LC-MS/MS) analysis. For peptide identification, we used a donor-specific V_H database comprising 98,413 unique high-quality sequences found in the natively paired V_H/V_L repertoire [in which an 850-base pair (bp) linked V_H/V_L amplicon was obtained using a single-cell emulsion method] from 845,000 peripheral B cells (20–22).

Using stringent data-filtering protocols (19), we identified high-confidence peptide-spectrum matches (PSMs) from HCDR3 peptides and used their LC peak intensities for relative quantification. We have previously demonstrated that ~80% of all HCDR3 peptides within a sample are identified in this manner (detection limit of about 0.4 ng/ml), and peak intensities correlated well with absolute peptide concentrations (17, 19).

Remarkably, we found that the MPER-specific plasma antibody repertoire consisted of three plasma Ig clonotypes (V_H sequences having the same germline V and J genes and 85% amino acid identity in the HCDR3), each of which used the same VDJ (V_H3-15 , D_H3-3 , and J_H6) as the DH511 clonal lineage (table S5). Clonotype IV comprised 95% of the total intensity of HCDR3 peptides detected in the MPER-specific antibody repertoire (i.e., in antibodies eluted after MPER peptide affinity chromatography); detection of HCDR1 and HCDR2 peptides unique to clonotype IV provided further support for the prevalence of this antibody in CH0210 plasma (table S6). Plasma clonotype II, which included memory B cell antibodies DH511.2, DH511.4, and DH511.5 upon phylogenetic analysis, and plasma clonotype III were detected at 4 and 1% relative abundance in plasma, respectively (Fig. 1F). Each of the three DH511 plasma clonotypes had HCDR3 lengths of 23 to 24 amino acids and V_H gene mutation rates of 11 to 20% (table S5). Neither MPER bnAb DH517 nor DH511 clonotype I (Fig. 1F), which includes DH511.1, DH511.3, and DH511.6 bnAbs, was detected in plasma. However, we demonstrated that recombinant DH517 as well as DH511.1, DH511.3, and DH511.6 antibodies were readily detectable by MS, indicating that their absence from the CH0210 plasma was not a technical artifact of LC-MS/MS proteomic analysis.

Using the proteomically identified HCDR3 sequences, we searched the native V_H/V_L sequence database of 64,389 sequences to determine full-length V_H/V_L sequences belonging

to each clonotype (table S5). For plasma antibody clonotypes with multiple V_H/V_L somatic variants, the two most frequent variants, as quantified by the number of sequencing –25 belonging to these clonotypes shared the same V and J gene identity (IGKV1-39 and IGKJ2) as did the light chains of the DH511 clonal lineage isolated by memory B cell single-cell sorting. Of the six plasma mAbs (designated DH511.7P to DH511.12P, with “P” indicating plasma origin), DH511.11P and DH511.12P demonstrated the most potent neutralizing activity against a panel of four HIV-1 isolates (table S7). In a panel of 208 HIV-1 isolates, DH511.11P and DH511.12P had slightly increased breadth and potency compared with DH511.2 [207 of 208 (99.5%) of the isolates tested] but were also slightly less potent than 10E8 (median IC_{50} : 0.8 μ g/ml for DH511.11P and 0.7 μ g/ml for DH511.12P versus 1.0 μ g/ml for DH511.2 and 0.4 μ g/ml for 10E8) (table S8).

Engineered bnAb for enhanced potency

Thirty-five chimeric mAbs were produced by swapping the heavy and light chains of DH511.2 with those of plasma DH511 lineage members. One chimeric mAb, DH511.2_K3 (composed of the memory B cell DH511.2 heavy chain with the light chain of plasma-derived DH511.8P), showed greater breadth and potency compared with 10E8 (table S9). DH511.2_K3 neutralized 206 of 208 (99%) global isolates (median IC_{50} : 0.37 μ g/ml for DH511.2_K3 and 0.39 μ g/ml for 10E8) (table S10) and neutralized 100% of 100 primary clade C HIV-1 isolates (IC_{50} , <50 μ g/ml), displaying both greater breadth and potency than 10E8 in this panel [10E8 breadth, 97% (IC_{50} , <25 μ g/ml); IC_{50} : 0.36 μ g/ml for DH511.2_K3 and 0.5 μ g/ml for 10E8] (table S11).

Structural analysis of memory B cell, plasma, and chimeric DH511 lineage bnAbs

Similar to the epitopes recognized by 4E10 and 10E8 (1), enzyme-linked immunosorbent assay (ELISA) analysis revealed that DH511 lineage antibodies derived from B memory cells or plasma were sensitive to alanine mutations at Asn671_{gp41} and Trp672_{gp41} but, unlike 4E10 and 10E8, were also sensitive to Asp674Ala_{gp41} and, to a lesser extent, to Leu679Ala_{gp41} mutations (fig. S1 and table S12). In contrast, the DH517 bnAb had a distinct footprint comprising amino acids in both the proximal and distal MPER (fig. S1). Neutralization activity of DH511.1 to DH511.6, DH511.11P, DH511.12P, and DH511.2_K3 mAbs against clade C COT6.15 Env pseudoviruses bearing alanine substitutions across the MPER (table S13) (23, 24) demonstrated neutralization sensitivity to Env mutations at Phe673Ala_{gp41}, Asp674Ala_{gp41}, and Asp674Ser_{gp41}, with the most prominent resistance observed against the Trp672Ala_{gp41} mutant virus (table S14). 10E8 was weakly sensitive in neutralization to Asp674Ala_{gp41} mutation as well.

Crystal structures of the antigen-binding fragments (Fab) of the distal MPER bnAb DH511.1 in complex with a peptide spanning the full gp41 MPER (residues 656 to 683) (25), of the DH511.2 antibody in complex with gp41 peptides spanning residues 662 to 683 and 670 to 683, and of the unliganded variant DH511.4 were determined at resolutions of 2.7, 2.6, 2.2, and 1.5 Å, respectively (Fig. 2, figs. S2 and S3, and tables S15 and S16). Both memory B cell-derived DH511.1 and DH511.2 recognized an α -helical conformation of the distal portion of the gp41 MPER (residues 671 to 683) (Fig. 2A), similar to the conformation recognized by neutralizing antibodies 10E8 and 4E10 (Fig. 2B), with Ca root mean square

deviations (RMSDs) of $<0.46 \text{ \AA}$ for this region across all structures. An extended conformation of gp41 MPER was observed between residues 662 and 670 in both the DH511.1 and DH511.2 structures, and in the case of DH511.1, an additional α helix was observed between residues 656 and 661, which was present at a lattice contact. Overall, the highest degree of structural homology for bound MPER occurred between gp41 residues 668 and 683, with a C α RMSD of 0.39 \AA (Fig. 2, A and C). Interactions between DH511.1 and DH511.2 and gp41 MPER were mediated exclusively by their heavy chains, with a contact interface of 674 to 751 \AA^2 on the antibodies and of 773 to 779 \AA^2 on gp41 (table S17). V_H3–15–encoded regions accounted for 45 to 50% of the interface with gp41, and HCDR3 loops accounted for 50% or more of the remaining interface (Figs. 2C and 3A and tables S17 and S18). gp41 residues Asn671_{gp41}, Trp672_{gp41}, Asp674_{gp41}, and Leu679_{gp41}, for which antibody binding was ablated or reduced when mutated to alanine, were all observed at the antibody interface (Fig. 2C and tables S18 and S19).

Crystal structures of plasma-derived DH511.11P and DH511.12P Fabs were determined in complex with a peptide spanning gp41 MPER residues 662 to 683 at resolutions of 2.47 and 1.88 \AA , respectively (Fig. 2, F and G, and tables S15 and S16). Both plasma-derived variants recognized a conformation of MPER similar to that recognized by memory B cell–derived DH511.1 and DH511.2, adopting an α helix between residues 671 and 683 and an extended conformation between residues 662 and 670. Despite a ~ 26 to 28% sequence divergence between the V_H regions of the plasma and memory B cell–derived variants, their respective structures were highly homologous. C α atom superpositions yielded RMSDs of between 0.7 to 1.6 \AA for their full light and heavy chain variable regions, and of $\sim 0.36 \text{ \AA}$ for their bound peptides. Interactions between DH511.11P and DH511.12P and gp41 were mediated exclusively by their heavy chains, similar to DH511.1 and DH511.2, with contact interfaces of 605 to 650 \AA^2 on the antibodies and 669 to 680 \AA^2 on gp41 (Fig. 2 and table S17). The plasma-derived variants recognized the same distal gp41 MPER residues (between 668 and 683) as those recognized by memory B cell–derived variants, although some interactions, such as with Asp674_{gp41}, were mediated through different sets of antibody residues (Fig. 2, C and G, and tables S18 and S19).

Comparison of the directions of approach of antibodies DH511.1, DH511.2, 10E8, and 4E10 to gp41 MPER, as defined by an axis drawn from a spatial position midway between the variable region disulfide bonds to the C α atom of residue Phe673_{gp41}, revealed that all three antibody lineages approached distal MPER from generally similar directions (Fig. 2E). Pair-wise comparisons of directions of approach relative to DH511.1 yielded angular differences of 4.7° , 13.4° , and 25.2° for antibodies DH511.2, 10E8, and 4E10, respectively (Fig. 2E). Whereas the DH511 lineage closely resembled 10E8 in its approach to the epitope, a rotational shift of $\sim 54^\circ$ around their relative directional axes was observed between the two lineages (Fig. 2, A and B), as evident in the rotation of their respective gp41 interfaces (Fig. 3A). Despite this rotation, five common V_H3–15 residue positions were nonetheless involved in interactions with gp41 in both lineages: residues 28, 31, and 33 within the HCDR1 and residues 52c and 53 within the HCDR2 (Figs. 2, C and D, and 3, A and B).

The crystal structure of the chimeric plasma/memory B cell bnAb DH511.2_K3 was determined at a resolution of 1.76 \AA in complex with a peptide spanning gp41 MPER

residues 670 to 683. The structure revealed that DH511.2_K3 recognized a conformation of gp41 MPER similar to that recognized by DH511.2 (C α RMSD of 0.23 Å) (Fig. 2, H and I, and tables S15 and S16), mediated by its structurally conserved common heavy chain with DH511.2 (C α RMSD of 0.39 Å). As in the case of DH511.2, the interface between DH511.2_K3 and gp41 was mediated exclusively by the heavy chain, burying surface areas of 667 and 760 Å² on the antibody and peptide, respectively, and maintaining an almost identical set of residue contacts with gp41 (Fig. 3B and tables S17 to S19). A large conformational shift was observed in the light chain LCDR3 loop of DH511.2_K3 (Fig. 2J), although its role in DH511.2_K3's enhanced potency is currently unknown.

A signature amino acid was identified at position 671 that was statistically strongly associated with viruses that were sensitive to neutralization by DH511 bnAbs (DH511.2, DH511.11P, DH511.12P, and DH511.2_K3), but not neutralized by 10E8. Both antibodies are broadly cross-reactive, and there were only three Env pseudoviruses in the global panel (tables S3, S8, and S10) sensitive to the DH511 lineage and 10E8-resistant. In the clade C panel (table S4), there were four viruses with this phenotype. The signature was identified using a phylogenetically corrected contingency analysis, scanning the full Env protein alignment to identify any amino acids associated with DH511's increased breadth (26, 27), and we required a q value (false discovery rate) of <0.2 (26) to be deemed of interest. Both viruses with Asn and Ser at position 671 were sensitive to both antibodies, whereas DH511 sensitivity and 10E8 resistance were significantly associated with a Thr at position 671 [P = 0.000025, q = 0.004 for the M group global panel data; P = 0.000038, q = 0.046 for the clade C, based on IC₈₀ sensitivity; the IC₅₀ sensitivity was also highly significant]. The specific 10E8 resistance conferred by Thr⁶⁷¹ was supported by structural modeling, which showed that the interaction of the two antibodies in the immediate vicinity of Env 671 is very distinctive and that a Thr substitution resulted in a structural clash with 10E8 that was not evident with DH511 bnAbs, whereas Asn⁶⁷¹ and Ser⁶⁷¹ were compatible with both bnAbs (Fig. 4). An earlier study showed that a substitution of Ala at 671 can confer resistance to 10E8 (1). Whereas viruses that were resistant to 10E8 and sensitive to DH511 bnAbs carried the Thr⁶⁷¹ substitution, it is interesting to note that 13 viruses that carried Thr⁶⁷¹ remained sensitive to 10E8, suggesting that other mutations in Env can also mitigate a clash at Thr⁶⁷¹.

DH511 clonal lineage development and immunogen design

A maximum likelihood phylogenetic tree was constructed from V_H/V_L natively paired memory B cell VDJ sequences recovered from single-cell sorting to infer the UCA of clone DH511 and six intermediate antibodies (I1 to I6) (Fig. 1B). A global panel (28) of 12 HIV-1 isolates was used to assess the development of neutralization breadth in the DH511 clonal lineage. None of the isolates were neutralized by the UCA or I6 antibody that was most closely related to the DH511 UCA. Antibody I2, with only 6.1% V_H mutations, acquired the ability to neutralize 12 of 12 isolates (table S20). Analysis of a panel of MPER peptides did not reveal constructs that bound with measurable affinity to the UCA (fig. S4). Rather, DH511 lineage member binding to MPER antigens at detectable affinity was acquired after the I6 stage of maturation. Acquisition of breadth in the DH511 clone was associated with the accumulation of somatic mutations and binding affinity to the distal MPER peptide

epitope (fig. S4). However, in Luminex assay and ELISA, the DH511 UCA did react with U1 small nuclear RNP (U1-snRNP), and in protein microarray assay, the DH511 UCA was both polyreactive and autoreactive with a number of proteins (table S21). Analysis of four recombinant RNP subunit proteins demonstrated DH511 UCA reactivity with subunit A of RNP and no reaction with B/B', C, or 68/70 kDa RNP subunits (fig. S5). Surface plasmon resonance analysis indicated the K_d of the DH511 UCA for RNP subunit A to be 0.84 μM (fig. S5). An amino acid alignment of HIV-1 Env gp41 and U1-snRNP A showed no regions of sequence similarity (fig. S6); structural comparison of U1-snRNP A and the MPER region bound by the DH511 lineage was not possible because only the N-terminal recognition motif domain of the U1-snRNP A crystal structure has been solved [Protein Data Bank (PDB): 3PGW] (29). The remainder of the DH511 lineage members had varying degrees of polyreactivity/autoreactivity, suggesting that similar to other MPER bnAb lineages, DH511-like lineages will be subject to immune tolerance control in the setting of vaccination (table S21) (4, 30, 31). Thus, one hypothesis is that the distal MPER bnAb DH511 clonal lineage UCA may have been initiated by self-antigens, and HIV-1 gp41 distal MPER antigens engaged later stages of the bnAb lineage after intermediate antibody I6 (32–34).

Mechanism of distal MPER bnAb interaction with virions

The binding of gp41 bnAbs 2F5 and 4E10 to the gp41-lipid complex has been proposed as a sequential two-step process, in which encountering the lipid membrane first takes place to aid in docking of the antibody with the transiently exposed gp41 intermediate-neutralizing epitope during the virion-host cell fusion process (35–37). Both DH511.2 and 10E8 weakly bound to bare liposomes but bound to MPER peptide liposomes (35, 37) in a two-step conformational change model that involved linked interactions, in which the mAbs initially form an encounter complex with the lipid and solvent exposed residues followed by the formation of a stable complex with the complete MPER epitope (Fig. 5). Thus, the mechanism of binding of both DH511.2 and 10E8 to MPER peptide in the context of lipids was similar to each other and similar to the mechanism previously reported for proximal MPER bnAb 2F5 and the highly polyreactive distal MPER bnAb 4E10 (25, 31, 35, 36). The bnAbs 10E8 and DH511.2 also captured infectious virions and bound GCN4 gp41-inter, a construct that mimics the extended prehairpin intermediate conformation of gp41 (figs. S7 and S8) (10, 38). Both early and late members of the DH511 lineage bound directly to GCN4 gp41-inter (fig. S8). Thus, the DH511 distal MPER bnAbs and the 10E8 bnAb bound both to the prefusion intermediate form of gp41 on infectious virions and to the gp41 intermediate form that is present after receptor-mediated activation of Env (37–39).

To determine the impact of timing of the gp41 intermediate epitope exposure on HIV-1 neutralization (40), we compared the window of time in which bnAbs DH511.2, 10E8, and 4E10 could neutralize the tier 2 HIV-1 strain B.BG1168 after virus addition to TZM-bl cells. The half-life of neutralization for DH511.2 ($t_{1/2} = 26.8 \pm 2.3$ min) was the same as that for bnAbs 10E8 ($t_{1/2} = 25.6 \pm 2.5$ min) and 4E10 ($t_{1/2} = 28.2 \pm 3.5$ min) and similar to the half-life of fusion inhibition by the gp41 intermediate mimic T20 ($t_{1/2} = 20.2 \pm 0.5$ min) (Fig. 6) (40). These results demonstrated that for neutralization, DH511.2 recognized a transiently exposed intermediate state of gp41 (38).

DISCUSSION

Here, we report the isolation and structural, biochemical, and functional characterization of broad and potent HIV-1 gp41 bnAb DH511 clonal lineage from both memory B cells and plasma. The memory B cell repertoire contains multiple specificities of antibodies reflective of an individual's immune history (41), whereas primary contributors to plasma antibodies are long- and short-lived plasma cells (18). There is indirect evidence that, at least for non-HIV-1 antigens such as influenza (42) and West Nile virus (43), a fraction of the antibodies encoded by antigen-specific memory B cells may be present in the serum at physiologically relevant concentrations, that is, at concentrations comparable to the antigen/antibody dissociation constant (K_d) values. In this study, we demonstrated that class-switched memory B cells and plasma antibodies shared some of the clonal lineage members of a potent and broadly neutralizing distal MPER bnAb. The relationship of the HIV-1-specific memory B cell and plasma antibody pools is complicated by HIV-1 infection-mediated damage of B cells, with disruption of the germinal center in the earliest stages of infection (44), and the accumulation of Fc receptor-like 4-positive memory B cells in chronic infection (45). Here, we show that blood plasma can be a rich source for the identification of potent bnAbs for recombinant antibody production and for constructing chimeric antibodies for enhancing antibody potency and breadth.

Both proximal MPER (2F5) and distal MPER (4E10) antibodies bind in a two-step process to the gp41 intermediate conformation that is induced after CD4 receptor-mediated Env activation (35, 36), and the epitope on virion Env of both 2F5 and 4E10 also involves the virion membrane (36). Irimia *et al.* (46) have demonstrated lipid as an integral component of the 4E10 epitope by crystallography.

It was of interest that 10E8 and DH511 mAbs similarly bound to HIV-1 MPER in the context of lipids (Fig. 5), and unlike the proximal MPER antibody 2F5, the distal MPER bnAbs DH511, 4E10, and 10E8 also captured infectious virions (fig. S7). These data demonstrated that distal MPER-targeting bnAbs bind to lipid and to an epitope on the prefusion conformation of Env gp41 before CD4-induced Env activation, a notion recently suggested by a cryo-electron microscopy structure of a membrane-bound HIV-1 trimer (47).

A limitation of this study is the lack of longitudinal samples from donor CH0210, who was identified during chronic HIV-1 infection, thus precluding detailed analysis of the emergence and maturation of MPER-directed antibody lineages from the time of HIV-1 infection. Such information could delineate MPER antibody-virus coevolution events and inform vaccine design strategies for the induction of such bnAbs. Additionally, we note that LC-MS/MS proteomics may somewhat underestimate the clonal diversity of the plasma MPER-specific antibody repertoire.

Finally, both 2F5 and 4E10 MPER bnAbs have been found to be limited in their induction by immune tolerance mechanisms (4–7). In the case of the 2F5 bnAb against the proximal MPER bnAb epitope, reactivity to both a host protein (kynureninase) and to host lipids limit 2F5-like antibody induction (31, 48). In primates, tolerance could be broken for the induction of 2F5 epitope antibodies that cross-react with kynureninase, but the induction of

lipid-reactive antibodies with hydrophobic HCDR3s remained strongly disfavored (31). Here, we found that the DH511 UCA and several other bnAb lineage members were polyreactive (table S21). We have previously shown HIV-1 antibody clonal lineage evolution from preexisting polyreactive antibody lineages selected by host or environmental antigens (32–34). The control of other proximal (2F5) and distal (4E10) MPER bnAb induction by central and peripheral tolerance mechanisms (4) suggests that the use of MPER immunogens that engage a preexisting antibody lineage induced by host antigens (32–34) in a vaccine formulation designed to transiently limit immune tolerance mechanisms (49) will be required for distal MPER bnAb induction.

MATERIALS AND METHODS

Study design

The purpose of this study was to isolate new distal MPER bnAbs and to study their ontogeny, breadth, and potency. Plasma samples from about 55 individuals with neutralization breadth (50) enrolled in the Center for HIV/AIDS Vaccine Immunology (CHAVI) 001 nonblinded, non-randomized, observational study protocol at CHAVI clinical sites in South Africa, Tanzania, and Malawi were assayed for Env antibody specificities after informed consent was obtained under protocols approved by the Institutional Review Board of the Duke University Health System, the National Institutes of Health (NIH), and review boards of the clinical sites in South Africa, Tanzania, and Malawi (51). Individuals were included in the study group who were known to be chronically infected with HIV-1 and were not elite viral controllers. All participants were antiretroviral naïve at the time of enrollment. The clade distribution and other characteristics of the cohort have been reported (49). South African individual CH0210, who was chronically infected with a clade C virus for an unknown period at the time of enrollment, was selected for bnAb isolation because of the presence of high levels of distal MPER bnAb neutralizing activity (12). CH0210 was only one of four such individuals identified with distal MPER bnAb specificity of the CHAVI 001 individuals studied, and the one individual of the four from whom potent bnAbs could be isolated. The DH511 bnAb lineage was isolated from CH0210 PBMCs and plasma collected at 8 weeks after study enrollment, where the viral load was 5180 copies/ml and the CD4 T cell count was unknown.

Epitope mapping and neutralization-based epitope prediction analysis

CH0210 plasma was assayed for neutralization breadth using mapping and computational methods for epitope prediction (11, 52). Anti-MPER bnAb activity was detected using two assays: plasma neutralization of the HIV-2/HIV-1 MPER chimeric pseudovirus C1C and plasma adsorption with MPER peptide-coated magnetic beads, followed by testing of adsorbed plasmas for reduction of neutralization activity, as described previously (53). A neutralization fingerprinting method for mapping the epitopes targeted by polyclonal antibody responses (11, 52) was used to delineate the specificities mediating breadth against a panel of 21 diverse HIV-1 strains. The resulting linear coefficients on a scale of 0 to 1 from the computational procedure were used to predict the relative prevalence of each of the reference antibody specificities in donor CH0210 plasma.

Antigen-specific single memory B cell sorting

Fluorescently labeled MPER peptide tetramer probes were generated using biotinylated MPR.03 peptide (KKKNEQELLELDKWASLWN-WFDITNWLWYIRKKK-biotin) (CPC Scientific Inc.) conjugated to fluorophore-labeled streptavidins, yielding a tetramer with four MPER epitopes for surface Ig cross-linking (13). PBMCs (11.5 million) from donor CH0210 were stained with MPR.03–Alexa Fluor 647 and MPR.03–Brilliant Violet 421 peptide tetramers and a cocktail of antibodies to identify MPER-specific memory B cells: surface IgM [fluorescein isothiocyanate (FITC)], surface IgD [phycoerythrin (PE)], CD3 (PE–Cy5), CD16 (Brilliant Violet 570), CD235a (PE–Cy5), CD19 [allophycocyanin (APC)–Cy7] (BD Biosciences), CD14 (Brilliant Violet 605) (Invitrogen), CD27 (PE–Cy7), CD38 (APC–Alexa Fluor 700) (Beckman Coulter), and CD10 (ECD) (Beckman Coulter). Aqua blue vital dye (Invitrogen) was used to stain dead cells. Using a four-laser FACS Aria cell sorter and FACSDiva software (BD Biosciences), single cell–sorted MPR.03 double-positive CD16[−]CD14[−]CD3[−]CD235[−]CD19⁺IgD[−]/CD38^{all} memory B cells were flow sorted into individual wells of a 96-well plate containing reverse transcription (RT) reaction buffer [5 μl of 5′ first-strand complementary DNA (cDNA) buffer, 0.5 μl of RNaseOUT (Invitrogen), 1.25 μl of dithiothreitol (DTT), 0.0625 μl of IGEPAL CA-630 (Sigma), 13.25 μl of distilled H₂O (Invitrogen)]. Data were analyzed using the FlowJo software (Tree Star). Plates were stored at −80°C until polymerase chain reaction (PCR) was performed.

PCR amplification and expression of Ig genes

Ig genes were amplified from RNA of isolated cells by RT-PCR. For RT, 10 mM dNTPs (New England Biolabs), 3 μl of random hexamers at 150 ng/ml (GeneLink), and 1 μl of SuperScript III (Invitrogen) were added to each well and subjected to thermocycling under the following conditions: 42°C for 10 min, 25°C for 10 min, 50°C for 60 min, and 94°C for 5 min. IgH, Igκ, and Igλ variable region genes were separately amplified from the cDNA by nested PCR, using AmpliTaq Gold 360 Master Mix (Invitrogen) and heavy chain (54) and light chain gene-specific primers, as previously described (55). PCR amplicons were purified and sequenced, and V_HDJ_H and V_LJ_L genes, mutation frequencies, and CDR3 lengths were determined using the Cloanlyst software (56). Clonal relatedness and inference of the UCA and intermediate antibodies were determined by computational methods as described previously (57–59). Maximum likelihood phylogenetic trees were constructed from V(D)J sequences using the Phylogeny Inference Package (PHYLIP) (version 3.69) (60). Transient small-scale expression of antibodies was achieved by overlapping PCR assembly of variable heavy and light chain gene pairs into IgH, Igκ, and Igλ linear expression cassettes for production of full-length IgG1 mAbs by transfection into 293T cells, as described previously (55). Supernatants were screened for HIV-1 Env binding by ELISA and neutralization activity in TZM-bl cells. For large-scale antibody production, antibody variable heavy chain and light chain genes were de novo synthesized (GenScript), cloned into pcDNA3.1 expression vectors containing the constant regions of IgG1 (55), and cotransfected at equal ratios in Expi293i cells using ExpiFectamine 293 transfection reagents (Thermo Fisher Scientific) according to the manufacturer's instructions. Culture supernatants were harvested and concentrated after 4 to 5 days of incubation at 37°C and 8% CO₂, followed by affinity purification by protein A column (Pierce, Thermo Fisher

Scientific). Antibody purity was evaluated by SDS–polyacrylamide gel electrophoresis and Coomassie Blue staining for heavy and light chains of the appropriate size.

The recovered antibodies were named by assigning the lineage designation “DH511,” followed by a specific antibody number “x” (referred to as DH511.“x”), allowing assignment of unique identifier for each clonal lineage member. Antibodies isolated from donor CH0210 plasma (as described in the methods below) were designated DH511.x.“P,” with “P” indicating plasma origin.

High-throughput paired V_H/V_L sequencing of Ig transcripts and proteomic analysis of serum IgG

Materials and reagents—Protein G Plus agarose, NeutrAvidin agarose, immobilized pepsin resin, and HyperSep SpinTip C18 columns (C18 Spin Tips) were acquired from Pierce (Thermo Fisher Scientific). Tris-hydrochloride (tris-HCl), ammonium bicarbonate (NH_4HCO_3), 2,2,2-trifluoroethanol (TFE), DTT, and iodoacetamide (IAM) were obtained from Sigma-Aldrich. LC-MS–grade water, acetonitrile (ACN), and formic acid were purchased from EMD.

Isolation of total B cells: Frozen PBMCs (10 million cells in 1 ml) were thawed at 37°C; resuspended in 50 ml of RPMI 1640 (Lonza) supplemented with 10% fetal bovine serum, 1× nonessential amino acids, 1× sodium pyruvate, 1× glutamine, 1× penicillin/streptomycin, and deoxyribonuclease I (20 U/ml); and recovered via centrifugation (300g for 10 min at 20°C). The cells were then resuspended in 4 ml of RPMI and allowed to recover at 37°C for 30 min. The cells were diluted with 10 ml of cold MACS buffer [phosphate-buffered saline (PBS) supplemented with 0.5% bovine serum albumin and 2 mM EDTA], collected by centrifugation (300g for 10 min at 4°C), and depleted of non-B cells using the Human Memory B Cell Isolation Kit with an LD column (Miltenyi Biotec) as per the manufacturer’s instructions. This yielded 400,000 to 500,000 B cells per vial.

Amplification of the paired V_H/V_L repertoire—The paired V_H and V_L sequences were determined using a custom-designed axisymmetric flow–focusing device (22) that is composed of three concentric tubes. Total B cells were suspended in 6 ml of cold PBS and passed through the innermost tube at a rate of 0.5 ml/min. Oligo-d(T)₂₅ magnetic beads (1 μm in diameter at a concentration of 45 μl of beads per milliliter of solution; NEB) were washed, subjected to focused ultrasonication (Covaris) to dissociate any aggregates, resuspended in 6 ml of lysis buffer [100 mM tris-HCl (pH 7.5), 500 mM LiCl, 10 mM EDTA, 1% lithium dodecyl sulfate (LiDS), 5 mM DTT], and passed through the middle tube at a rate of 0.5 ml/min. The outer tubing contained an oil phase (mineral oil containing 4.5% Span-80, 0.4% Tween 80, and 0.05% Triton X-100; Sigma-Aldrich) flowing at 3 ml/min. The cells, beads, and lysis buffer were emulsified as they passed through a custom-designed 120-μm-diameter orifice and were subsequently collected in 2-ml microcentrifuge tubes. Each tube was inverted several times, incubated at 20°C for 3 min, and then placed on ice. After the collection phase, emulsions were pooled into 50-ml conicals and centrifuged (4000g for 5 min at 4°C). The mineral oil (upper phase) was decanted, and the emulsions (bottom phase) were broken with water-saturated cold diethyl ether (Fisher). Magnetic beads

were recovered after a second centrifugation step (4000g for 5 min at 4°C) and resuspended in 1 ml of cold buffer 1 [100 mM tris (pH 7.5), 500 mM LiCl, 10 mM EDTA, 1% LiDS, 5 mM DTT]. The beads were then serially pelleted using a magnetic rack and washed with the following buffers: 1 ml of lysis buffer, 1 ml of buffer 1, and 0.5 ml of buffer 2 [20 mM tris (pH 7.5), 50 mM KCl, 3 mM MgCl]. The beads were split into two aliquots, and each was then pelleted one final time and resuspended in an RT-PCR mixture (22) containing V_H and V_L framework region 1 (FR1) linkage primers or V_H and V_L leader peptide (LP) linkage primers (table S22, A and B). The RT-PCR mixtures were then added dropwise to 9 ml of chilled oil phase in an IKA dispersing tube (DT-20, VWR) and emulsified using an emulsion dispersing apparatus (ULTRA-TURRAX Tube Drive; IKA) for 5 min. The emulsions were aliquoted into 96-well PCR plates (100 µl per well) and subjected to RT-PCR under the following conditions: 30 min at 55°C followed by 2 min at 94°C; 4 cycles at 94°C for 30 s, 50°C for 30 s, and 72°C for 2 min; 4 cycles at 94°C for 30 s, 55°C for 30 s, and 72°C for 2 min; 32 cycles at 94°C for 30 s, 60°C for 30 s, and 72°C for 2 min; and 7 min at 72°C; held at 4°C.

After RT-PCR, the emulsions were collected in 2-ml microcentrifuge tubes and centrifuged (16,000g for 10 min at 20°C). The mineral oil (upper phase) was decanted, and water-saturated ether was used to break the emulsions. The aqueous phase (containing the DNA) was extracted three times by sequentially adding ether, centrifuging the samples (16,000g for 30 s at 20°C), and removing the upper ether phase. Trace amounts of ether were removed using SpeedVac for 30 min at 20°C. The DNA amplicons were purified using a silica spin column (Zymo-Spin I, Zymo Research), according to the manufacturer's instructions, and eluted in 40 µl of H₂O. The two samples were then amplified through a nested PCR (see table S22C for primers) using Platinum Taq (Life Technologies) under the following conditions: (FR1 primer-derived sample) 2 min at 94°C, 32 cycles of 94°C for 30 s, 62°C for 30 s, 72°C for 20 s; 72°C for 7 min; held at 4°C; (LP primer-derived sample) 2 min at 94°C, 27 cycles of 94°C for 30 s, 62°C for 30 s, 72°C for 20 s; 72°C for 7 min; held at 4°C. The amplicons, about 850 bp in length, were gel-purified from 1% agarose using a gel extraction kit (Zymo Research), according to the manufacturer's instructions, and eluted in 20 µl of H₂O.

To determine the full-length V_H and V_L reads for antibody expression studies, we subjected the paired amplicon to an additional PCR using NEBNext high-fidelity polymerase (NEB) to specifically amplify the full V_H chain and the full V_L chain separately in addition to the paired chains (note: the paired reads sequence the entire J and D regions and the fragment of the V regions spanning FR2 to CDR3). Each sample was split into five reactions and subjected to the following PCR conditions: 30 s at 98°C, *X* cycles of 98°C for 10 s, 62°C for 30 s, 72°C for *Y* s; 72°C for 7 min; held at 4°C (see table S22D for the PCR conditions and table S22E for the primer sequences). Last, these sequences were amplified one final time with TruSeq barcode-compatible barcoding primers following the protocol shown in table S22F, gel-purified from 1% agarose using a gel purification kit according to the manufacturer's instructions, and submitted for paired-end Illumina next-generation sequencing (NGS).

Bioinformatic analysis of NGS data—Raw 2×300 MiSeq reads were quality-filtered (minimum Phred score of 20 over half of the nucleotide sequence) and submitted to MiXCR (61) for CDR3 identification and gene annotation. Productive V_H and V_L reads were paired by Illumina MiSeq ID using a custom python script. Full-length V_H and V_L reads were stitched together using FLASH (62) and then quality-filtered. Full-length V_H and V_L constructs were designed by matching the paired HCDR3/LCDR3 nucleotide sequences to the respective CDR3 in the full-length V_H and V_L libraries.

Sample preparation and LC-MS/MS analysis—Plasma IgG from donor 0210 was purified by Protein G Plus agarose affinity chromatography, and $F(ab')_2$ fragments were generated by digestion with immobilized pepsin. Antigen-specific $F(ab')_2$ was isolated by affinity chromatography with the biotinylated MPER peptide coupled to NeutrAvidin agarose and eluted in 100 mM glycine (pH 2.7). The collected fractions were neutralized, and the protein-containing fractions were pooled and prepared for LC-MS/MS, as described previously (19). Briefly, protein samples were concentrated and resuspended in 50% (v/v) TFE, 50 mM NH_4HCO_3 , and 2.5 mM DTT and incubated at 55°C for 45 min. The reduced samples were then alkylated with IAM in the dark, at room temperature for 30 min. The reaction was quenched by addition of DTT, and the samples were diluted to 5% TFE and digested with trypsin (trypsin/protein ratio of 1:75 at 37°C for 5 hours). The digestion was stopped by adding formic acid to 1% (v/v). The samples were then concentrated by SpeedVac and resuspended in 5% ACN and 0.1% formic acid, and the peptides were washed on C18 Spin Tips according to the manufacturer's protocol. Subsequently, the peptides were separated by reversed-phase chromatography (Dionex UltiMate 3000 RSLCnano System with Dionex Acclaim PepMap RSLC C18 column, Thermo Scientific) and analyzed online by nano-electrospray ionization-MS/MS on Orbitrap Velos Pro (Thermo Scientific). MS1 scans were collected in the orbitrap at a resolution of 60,000 Å, and the ions with $>+1$ charge were fragmented by collision-induced dissociation with up to 20 MS2 spectra collected per MS1.

Computational interpretation of peptide mass spectra—Full-length V_H and V_L sequencing data (see above) were submitted to the IMGT/HighV-QUEST tool (63) for annotation, and unique full-length V_H sequences were clustered into clonotypes according to their HCDR3 sequences with a cutoff of 85% identity as described previously (64). The sample-specific target protein sequence database was constructed from the full-length V_H and V_L sequences mentioned above (≥ 2 reads), Ensembl human protein-coding sequences, and common contaminants (maxquant.org). The spectra were then searched against this database using SEQUEST (Proteome Discoverer 1.4, Thermo Scientific) with previously described settings (17). The resulting PSMs were filtered with Percolator (Proteome Discoverer 1.4) to control false discovery rates to $<1\%$; the average mass deviation (AMD) was calculated for all high-confidence PSMs, and peptides with an AMD of <1.5 parts per million were kept for the final data set. Informative peptides, as defined previously (17), were grouped by their HCDR1, HCDR2, or HCDR3 association, and for each group, the abundances of the corresponding clonotypes were determined by the sum of the extracted ion chromatograms of the respective precursor ions.

Enzyme-linked immunosorbent assays

Binding of transiently transfected supernatants and mAbs to HIV-1 Env proteins and peptides was detected by ELISA. High-binding 384-well plates (Corning) were coated overnight at 4°C or for 2 hours at room temperature with HIV-1 protein or streptavidin (2 µg/ml) (for detection of binding to biotinylated peptides) in 0.1 M sodium bicarbonate (Sigma-Aldrich). U1 spliceosomal RNA U1-snRNP components A, B/B', C, and 68/70 kDa (SurModics) were coated at 60 ng per well. Plates were blocked for 1 hour at room temperature with assay diluent composed of PBS, 4% (w/v) whey protein (BiPro USA), 15% normal goat serum (Invitrogen), 0.5% Tween 20, and 0.05% sodium azide (Sigma-Aldrich), followed by a 1-hour incubation with antibody at a starting concentration of 100 µg/ml, serially diluted threefold. Horseradish peroxidase-conjugated goat anti-human IgG Fc antibody (Jackson ImmunoResearch Laboratories) was added to each well and incubated for 1 hour, after which plates were washed with PBS/0.1% Tween 20 and developed with SureBlue Reserve TMB One Component Microwell Peroxidase Substrate for 15 min (KPL). Development was stopped with 0.1 M HCl, and plates were read at 450 nm. Experiments were performed in duplicate, and results were reported as logarithm area under the curve (Log AUC). For epitope mapping, purified mAbs were screened as listed above against a panel of MPR.03 alanine-scanned peptides. Epitope positions were defined by MPR.03 alanine scan mutations that reduced the Log AUC by >50% compared with the wild-type peptide.

Neutralization assays

Neutralization assays were performed using HIV-1 Env pseudoviruses to infect TZM-bl cells as previously described (65, 66). A four-parameter hill slope equation was used to fit neutralization curves by nonlinear regression and for determination of maximum percent inhibition values. Titers were calculated as IC₅₀ and IC₈₀ and reported as the concentration of antibody causing a 50 or 80% reduction in relative luminescence units compared with virus control wells. Mapping of the MPER residues critical for neutralization was performed using a panel of alanine-scanned COT6.15 Env pseudoviruses, as described previously (23, 24).

Neutralization signature analysis

A computational approach was used to define neutralization signatures by analyzing Env sequences from viruses that were differentially sensitive to neutralization by DH511 lineage and 10E8 mAbs. Using a previously described maximum likelihood tree correction method (26, 27), we scanned amino acids at each position in a given Env to identify mutational patterns that correlated with susceptibility or resistance in a multiclade panel of 208 isolates or a panel of 200 early/acute clade C viruses. Sequences were aligned using Gene Cutter (www.hiv.lanl.gov) to identify signature sites, after which phylogenetic statistical correction methods were applied to account for founder effects that can lead to false-positive statistical associations (26). Associations were considered significant if *P* values were less than 0.05 and *q* values (false discovery rate after correction for multiple comparisons) were less than 0.2.

Modeling interactions of Env position 671 with 10E8 and DH511.2

We used the gp41 MPER peptide 10E8 cocrystal structure PDB 4G6F (1) and the peptide-DH511.2 cocrystal structure resolved in this work to model the interactions of Asn, Thr, and Ser at position 671 with 10E8 and DH511.2. Both the structures had Asn at 671, the most common amino acid at this position (671 is 72% N, 21% S, and 5.5% T in the global alignment at the HIV database). Using homology modeling, we modeled the presence of Thr and Ser at this position. We used the Mutagenesis tool in PyMOL, with default settings to generate these models, and used the top models for side chains in each case. For the 10E8 cocrystal structure, we also used CPHmodels web server (67) to model Ser and Thr at position 671, which provided almost identical models as PyMOL [*The PyMOL Molecular Graphics System, Version 1.8* (Schrodinger LLC, 2015)]. For understanding steric clashes, we analyzed the abovementioned structures and models in Visual Molecular Dynamics (VMD) (68) and used the default threshold of 1.4 Å around each heavy atom to render the protein surfaces.

Affinity and kinetics measurements of MPER peptide and MPER liposome binding

Surface plasmon resonance analysis of MPER peptide binding was performed on a Biacore S200 instrument (GE Healthcare) at 25°C, and data were analyzed using the BIAevaluation S200 software (BIAcore) as described previously (35). To determine the affinity, association, and dissociation rate constants of the DH511 clonal lineage to MPER, we coated biotinylated MPR.03 peptide on streptavidin sensors (SA sensor chip) at a density of 58 to 60 response units. DH511 lineage Fabs were injected over flow cells at increasing concentrations at a flow rate of 50 µl/min, with 5-min association and 10-min dissociation steps. Curves were blank SA surface-subtracted. Rate constants for MPR.03 peptide binding were measured using the “heterogeneous ligand” model and apparent equilibrium K_d derived using the faster component of the association and dissociation rates. U1-snRNP binding was measured by flowing it over DH511_UCA mAb, which was captured on an anti-human IgFc immobilized surface as described previously (35, 69), and K_d values were derived from steady-state affinity or from rate constants measured using global fitting to the langmuir 1:1 model. Peptide-liposome conjugates were generated with either MPER656 or MPER656.1-GTH1 peptides using an extrusion method (35) and analyzed by biolayer interferometry measurements using Octet RED96 (Forte-Bio) and binding rate constant derived after curve-fitting to a two-step encounter docking model, as described previously (31, 35). Forte-Bio Aminopropylsilane (APS) sensors were used to capture MPER liposomes, and antibodies were used at concentrations ranging from 10 to 200 µg/ml (10E8 and DH511.2) or from 5 to 80 µg/ml (4E10).

Polyreactivity/autoreactivity analysis

Antibody binding to a panel of nine autoantigens, including Sjögren’s syndrome antigen A (SSA), SSB, Smith antigen, RNP, scleroderma 70, Jo-1, double-stranded DNA, centromere B, and histone, was quantified by a Luminex-based AtheNA Multi-Lyte ANA assay (Zeus Scientific Inc.). Anti-cardiolipin reactivity was measured using a QUANTA Lite ACA IgG III ELISA kit (Nova Diagnostics) as per the manufacturer’s instructions, as previously described (70). Antibodies were assayed for reactivity to the human epithelial cell line

(HEp-2) by indirect immunofluorescence staining using the IFA ANA/Hep-2 Test System (Zeus Scientific) as per the manufacturer's protocol. Antibodies were diluted to 50 and 25 $\mu\text{g/ml}$ and scored negative or positive (1+ to 4+) at each dilution. Antibodies were also screened for binding to a panel of >9400 human proteins using a ProtoArray microarray (Invitrogen), according to the manufacturer's instructions and as described by Liu *et al.* (9). Briefly, the array was blocked and incubated on ice with HIV-1 antibody (2 $\mu\text{g/ml}$) or the isotype control antibody, human myeloma protein, 151K (Southern Biotech) for 90 min. Antibody binding was detected with anti-human IgG–Alexa 647 secondary antibody (1 $\mu\text{g/ml}$) (Invitrogen). Arrays were scanned using a GenePix 4000B scanner (Molecular Devices) at a wavelength of 635 nm and resolution of 10 μm , using 100% power and 650 gain. The fluorescence intensity of antibody binding was measured with the GenePix Pro 5.0 program (Molecular Devices).

Infectious virion capture assay

The capacity of DH511 lineage antibodies to capture functional virions was assessed using a previously described protein G column– based assay (71, 72) that distinguishes between capture of infectious and noninfectious virions. Immune complexes, formed by mixing mAbs with virions expressing either B. TRO.11 or transmitted founder C.CAP206 Envs, were absorbed by a Protein G MultiTrap 96-well plate (GE Healthcare Inc.). Infectious virions were quantified in the flow-through fraction by a TZM-bl infectivity assay. Total virions in the flow-through and captured fractions were measured by detection of viral RNA by HIV *gag* real-time RT-PCR. The percent infectious virion capture was calculated using the following equation: $[(100 - \text{flow-through infectivity})/\text{virus-only infectivity}] \times 100$.

Time course of DH511.2 neutralization

The time course of DH511.2 neutralization was determined using a post-attachment HIV-1– pseudotyped virus neutralization assay described previously (73). Inhibitory concentrations of DH511.2, 10E8, and 4E10 mAbs were added to TZM-bl cells incubated with B.BG1168 virus at different time intervals after infection. Infectivity was measured in relative light units.

Crystallization, structure determination, and structural analysis

Purified DH511.4 fragment of antigen binding (Fab) was set up in crystallization trials in an unliganded state against commercially available screens (Hampton Research, Qiagen) as vapor diffusion sitting drops robotically (Douglas Instruments Ltd.). Crystals of DH511.4 Fab (table S16) were obtained in a condition composed of 0.2 M disodium hydrogen phosphate and 20% PEG-3350 (polyethylene glycol, molecular weight 3350). These crystals were cryoprotected using mother liquor supplemented with ethylene glycol. Purified DH511.1, DH511.2, DH511.11P, DH511.12P, and DH511.2_K3 Fabs were set up in crystallization trials in complex with a panel of gp41 MPER peptides added at threefold or higher molar excess. For each complex, 576 initial conditions from commercially available screens (Hampton Research, Rigaku) were set up as vapor diffusion sitting drops robotically (TTP Labtech). Crystals of DH511.1 Fab in complex with gp41 MPER peptide residues 656 to 683 were obtained in a condition composed of 30% PEG-1500, whereas those of DH511.2 Fab in complex with peptides MPR.03.DN4 and MPR.03.DN14 were obtained in

30% PEG-1500, 10% isopropanol, 0.1 M CaCl₂, and 0.1 M imidazole (pH 6.5) and in 20% PEG-8000, 10% PEG-400, 0.5 M NaCl, and 0.1 M C₂H₃NaO₂ (pH 5.5), respectively. Crystals of DH511.11P and DH511.12P Fabs in complex with the gp41 MPER peptide MPR.03.DN4 were obtained in a condition comprising 4% isopropanol, 3% PEG-3350, 0.75 M NH₄SO₄, and 0.1 M C₂H₃NaO₂ (pH 4.5). Crystals of DH511.2_K3 Fab in complex with the gp41 MPER peptide MPR.03.DN14 were obtained in a condition comprising 7% isopropanol, 20% PEG-3350, and 0.2 M ammonium citrate (pH 4.5). Crystal hits were hand-optimized, and x-ray diffraction data were collected either without additional cryoprotectants or using mother liquor supplemented with 15% 2*R*,3*R*-butanediol. Data were processed with HKL-2000 (29). The unliganded DH511.4 Fab structure was solved by molecular replacement in Phaser (74) using, as search models, structures of antibody Fab fragments, which were matched by high sequence homology: the heavy chain of anti-HIV antibody 447-52D (PDB: 3GHB) (75) and the light chain of the human germline antibody 5-51/012 (PDB: 4KMT) (76). The DH511.1, DH511.2, DH511.11P, DH511.12P, and DH511.2_K3 complex structures were solved by molecular replacement using the unliganded DH511.4 Fab (for DH511.1) and subsequent DH511 lineage structures as search models in Phaser (74). All structures were refined using Phenix (77), combined with iterative model building in Coot (78). Interactive surfaces and structural alignments were determined using Pisa (79) and LSQKAB (80), respectively. All graphical images were prepared with PyMOL (PyMOL Molecular Graphics System). X-ray diffraction data were collected at SER CAT ID-22 or BM-22 beamlines of the Advanced Photon Source (Argonne, IL), under General User Proposal 44127 (G.O.) and as a supporting institution (Duke University).

Supplementary Material

Refer to Web version on PubMed Central for supplementary material.

Acknowledgments

We acknowledge J. F. Whitesides, M. Wang, Y. Yang, M. Jin, M. Cooper, E. Dunford, A. Hogan, A. Foulger, S. Arora, R. Reed, E. Friberg, J. A. Holland, H. Chen, J. Pritchett, G. Hernandez, T. C. Gurley, L. E. Stiegel, L. C. Armand, T. A. von Holle, K. E. Lloyd, C. Stolarchuk, H. Wright, E. Obremski, C. Vivian, L. Sutherland, S. Krasteva, D. Goodman, and Q. Zhou for expert technical assistance. We thank T. Travers for helpful discussions. We thank K. A. Soderberg, A. Sanchez, A. M. Trama, H. Bouton-Verville, A. Eaton, K. Greene, H. Gao, C. C. Labranche, and N. A. Doria-Rose for program management and/or assistance with neutralization assays.

Funding: This work was funded by the NIH, National Institute of Allergy and Infectious Diseases, Division of AIDS grant for the Duke Center for HIV/AIDS Vaccine Immunology and Immunogen Discovery (CHAVI-ID; UM1 AI 0100645); Collaboration for AIDS Vaccine Discovery grant from the Bill and Melinda Gates Foundation (OPP1115416 to B.F.H.); the Interdisciplinary Research Training Program in AIDS (T32 AI007392 to L.D.W. and G.D.T.); the Duke Center for AIDS Research (P30 AI 64518); Defense Threat Reduction Agency contract HDTRA1-12-C-0105 (to G.G.); and the Intramural Research Program of the Vaccine Research Center, National Institute of Allergy and Infectious Diseases. LC-MS/MS instrumentation at the University of Texas at Austin was supported by Cancer Prevention Research Institute of Texas grant RP100890. Use of the Advanced Photon Source was supported by the Office of Basic Energy Sciences, Office of Science, U.S. Department of Energy, under contract number W-31-109-Eng-38.

REFERENCES AND NOTES

1. Huang J, Ofek G, Laub L, Louder MK, Doria-Rose NA, Longo NS, Imamichi H, Bailer RT, Chakrabarti B, Sharma SK, Alam SM, Wang T, Yang Y, Zhang B, Migueles SA, Wyatt R, Haynes

- BF, Kwong PD, Mascola JR, Connors M. Broad and potent neutralization of HIV-1 by a gp41-specific human antibody. *Nature*. 2012; 491:406–412. [PubMed: 23151583]
2. Zwick MB, Labrijn AF, Wang M, Spelshauer C, Saphire EO, Binley JM, Moore JP, Stiegler G, Katinger H, Burton DR, Parren PWHI. Broadly neutralizing antibodies targeted to the membrane-proximal external region of human immunodeficiency virus type 1 glycoprotein gp41. *J. Virol*. 2001; 75:10892–10905. [PubMed: 11602729]
 3. Kwon YD, Georgiev IS, Ofek G, Zhang B, Asokan M, Bailer RT, Bao A, Caruso W, Chen X, Choe M, Druz A, Ko S-Y, Louder MK, McKee K, O'Dell S, Pegu A, Rudicell R, Shi W, Wang K, Yang Y, Alger M, Bender MF, Carlton K, Cooper JW, Blinn J, Eudailey J, Lloyd K, Parks R, Alam SM, Haynes BF, Padte NN, Yu J, Ho DD, Huang J, Connors M, Schwartz RM, Mascola JR, Kwong PD. Optimization of the solubility of HIV-1-neutralizing antibody 10E8 through somatic variation and structure-based design. *J. Virol*. 2016; 90:5899–5914. [PubMed: 27053554]
 4. Chen Y, Zhang J, Hwang K-K, Bouton-Verville H, Xia S-M, Newman A, Ouyang Y-B, Haynes BF, Verkoczy L. Common tolerance mechanisms, but distinct cross-reactivities associated with gp41 and lipids, limit production of HIV-1 broad neutralizing antibodies 2F5 and 4E10. *J. Immunol*. 2013; 191:1260–1275. [PubMed: 23825311]
 5. Doyle-Cooper C, Hudson KE, Cooper AB, Ota T, Skog P, Dawson PE, Zwick MB, Schief WR, Burton DR, Nemazee D. Immune tolerance negatively regulates B cells in knock-in mice expressing broadly neutralizing HIV antibody 4E10. *J. Immunol*. 2013; 191:3186–3191. [PubMed: 23940276]
 6. Verkoczy L, Diaz M, Holl TM, Ouyang Y-B, Bouton-Verville H, Alam SM, Liao H-X, Kelsoe G, Haynes BF. Autoreactivity in an HIV-1 broadly reactive neutralizing antibody variable region heavy chain induces immunologic tolerance. *Proc. Natl. Acad. Sci. U.S.A.* 2010; 107:181–186. [PubMed: 20018688]
 7. Verkoczy L, Chen Y, Bouton-Verville H, Zhang J, Diaz M, Hutchinson J, Ouyang Y-B, Alam SM, Holl TM, Hwang K-K, Kelsoe G, Haynes BF. Rescue of HIV-1 broad neutralizing antibody-expressing B cells in 2F5 V_H × V_L knockin mice reveals multiple tolerance controls. *J. Immunol*. 2011; 187:3785–3797. [PubMed: 21908739]
 8. Haynes BF, Fleming J, St Clair EW, Katinger H, Stiegler G, Kunert R, Robinson J, Scearce RM, Plonk K, Staats HF, Ortel TL, Liao HX, Alam SM. Cardioliipin polyspecific autoreactivity in two broadly neutralizing HIV-1 antibodies. *Science*. 2005; 308:1906–1908. [PubMed: 15860590]
 9. Liu M, Yang G, Wiehe K, Nicely NI, Vandergrift NA, Rountree W, Bonsignori M, Alam SM, Gao J, Haynes BF, Kelsoe G. Polyreactivity and autoreactivity among HIV-1 antibodies. *J. Virol*. 2015; 89:784–798. [PubMed: 25355869]
 10. Chen J, Frey G, Peng H, Rits-Volloch S, Garrity J, Seaman MS, Chen B. Mechanism of HIV-1 neutralization by antibodies targeting a membrane-proximal region of gp41. *J. Virol*. 2014; 88:1249–1258. [PubMed: 24227838]
 11. Georgiev IS, Doria-Rose NA, Zhou T, Kwon YD, Staube RP, Moquin S, Chuang G-Y, Louder MK, Schmidt SD, Altae-Tran HR, Bailer RT, McKee K, Nason M, O'Dell S, Ofek G, Pancera M, Srivatsan S, Shapiro L, Connors M, Migueles SA, Morris L, Nishimura Y, Martin MA, Mascola JR, Kwong PD. Delineating antibody recognition in polyclonal sera from patterns of HIV-1 isolate neutralization. *Science*. 2013; 340:751–756. [PubMed: 23661761]
 12. Pancera M, Zhou T, Druz A, Georgiev IS, Soto C, Gorman J, Huang J, Acharya P, Chuang G-Y, Ofek G, Stewart-Jones GBE, Stuckey J, Bailer RT, Joyce MG, Louder MK, Tumba N, Yang Y, Zhang B, Cohen MS, Haynes BF, Mascola JR, Morris L, Munro JB, Blanchard SC, Mothes W, Connors M, Kwong PD. Structure and immune recognition of trimeric pre-fusion HIV-1 Env. *Nature*. 2014; 514:455–461. [PubMed: 25296255]
 13. Morris L, Chen X, Alam M, Tomaras G, Zhang R, Marshall DJ, Chen B, Parks R, Foulger A, Jaeger F, Donathan M, Bilska M, Gray ES, Abdool Karim SS, Kepler TB, Whitesides J, Montefiori D, Moody MA, Liao H-X, Haynes BF. Isolation of a human anti-HIV gp41 membrane proximal region neutralizing antibody by antigen-specific single B cell sorting. *PLOS ONE*. 2011; 6:e23532. [PubMed: 21980336]
 14. Purtscher M, Trkola A, Gruber G, Buchacher A, Predl R, Steindl F, Tauer C, Berger R, Barrett N, Jungbauer A, Katinger H. A broadly neutralizing human monoclonal antibody against gp41 of human immunodeficiency virus type 1. *AIDS Res. Hum. Retrovir*. 1994; 10:1651–1658. [PubMed: 7888224]

15. Buchacher A, Predl R, Strutzenberger K, Steinfellner W, Trkola A, Purtscher M, Gruber G, Tauer C, Steindl F, Jungbauer A, Katinger H. Generation of human monoclonal antibodies against HIV-1 proteins; electrofusion and Epstein-Barr virus transformation for peripheral blood lymphocyte immortalization. *AIDS Res. Hum. Retrovir.* 1994; 10:359–369. [PubMed: 7520721]
16. Haynes BF, Moody MA, Verkoczy L, Kelsoe G, Alam SM. Antibody polyspecificity and neutralization of HIV-1: A hypothesis. *Hum. Antibodies.* 2005; 14:59–67. [PubMed: 16720975]
17. Lavinder JJ, Wine Y, Giesecke C, Ippolito GC, Horton AP, Lungu OI, Hoi KH, DeKosky BJ, Murrin EM, Wirth MM, Ellington AD, Dorner T, Marcotte EM, Boutz DR, Georgiou G. Identification and characterization of the constituent human serum antibodies elicited by vaccination. *Proc. Natl. Acad. Sci. U.S.A.* 2014; 111:2259–2264. [PubMed: 24469811]
18. Wine Y, Horton AP, Ippolito GC, Georgiou G. Serology in the 21st century: The molecular-level analysis of the serum antibody repertoire. *Curr. Opin. Immunol.* 2015; 35:89–97. [PubMed: 26172290]
19. Boutz DR, Horton AP, Wine Y, Lavinder JJ, Georgiou G, Marcotte EM. Proteomic identification of monoclonal antibodies from serum. *Anal. Chem.* 2014; 86:4758–4766. [PubMed: 24684310]
20. McDaniel JR, DeKosky BJ, Tanno H, Ellington AD, Georgiou G. Ultra-high-throughput sequencing of the immune receptor repertoire from millions of lymphocytes. *Nat. Protoc.* 2016; 11:429–442. [PubMed: 26844430]
21. DeKosky BJ, Ippolito GC, Deschner RP, Lavinder JJ, Wine Y, Rawlings BM, Varadarajan N, Giesecke C, Dörner T, Andrews SF, Wilson PC, Hunicke-Smith SP, Willson CG, Ellington AD, Georgiou G. High-throughput sequencing of the paired human immunoglobulin heavy and light chain repertoire. *Nat. Biotechnol.* 2013; 31:166–169. [PubMed: 23334449]
22. DeKosky BJ, Kojima T, Rodin A, Charab W, Ippolito GC, Ellington AD, Georgiou G. In-depth determination and analysis of the human paired heavy- and light-chain antibody repertoire. *Nat. Med.* 2015; 21:86–91. [PubMed: 25501908]
23. Gray ES, Madiga MC, Moore PL, Mlisana K, Abdool Karim SS, Binley JM, Shaw GM, Mascola JR, Morris L. Broad neutralization of human immunodeficiency virus type 1 mediated by plasma antibodies against the gp41 membrane proximal external region. *J. Virol.* 2009; 83:11265–11274. [PubMed: 19692477]
24. Gray ES, Meyers T, Gray G, Montefiori DC, Morris L. Insensitivity of paediatric HIV-1 subtype C viruses to broadly neutralising monoclonal antibodies raised against subtype B. *PLOS Med.* 2006; 3:e255. [PubMed: 16834457]
25. Dennison SM, Stewart SM, Stempel KC, Liao H-X, Haynes BF, Alam SM. Stable docking of neutralizing human immunodeficiency virus type 1 gp41 membrane-proximal external region monoclonal antibodies 2F5 and 4E10 is dependent on the membrane immersion depth of their epitope regions. *J. Virol.* 2009; 83:10211–10223. [PubMed: 19640992]
26. Bhattacharya T, Daniels M, Heckerman D, Foley B, Frahm N, Kadie C, Carlson J, Yusim K, McMahon B, Gaschen B, Mallal S, Mullins JI, Nickle DC, Herbeck J, Rousseau C, Learn GH, Miura T, Brander C, Walker B, Korber B. Founder effects in the assessment of HIV polymorphisms and HLA allele associations. *Science.* 2007; 315:1583–1586. [PubMed: 17363674]
27. Gnanakaran S, Daniels MG, Bhattacharya T, Lapedes AS, Sethi A, Li M, Tang H, Greene K, Gao H, Haynes BF, Cohen MS, Shaw GM, Seaman MS, Kumar A, Gao F, Montefiori DC, Korber B. Genetic signatures in the envelope glycoproteins of HIV-1 that associate with broadly neutralizing antibodies. *PLOS Comput. Biol.* 2010; 6:e1000955. [PubMed: 20949103]
28. deCamp A, Hraber P, Bailer RT, Seaman MS, Ochsenbauer C, Kappes J, Gottardo R, Edlefsen P, Self S, Tang H, Greene K, Gao H, Daniell X, Sarzotti-Kelsoe M, Gorny MK, Zolla-Pazner S, LaBranche CC, Mascola JR, Korber BT, Montefiori DC. Global panel of HIV-1 Env reference strains for standardized assessments of vaccine-elicited neutralizing antibodies. *J. Virol.* 2014; 88:2489–2507. [PubMed: 24352443]
29. Weber G, Trowitzsch S, Kastner B, Lührmann R, Wahl MC. Functional organization of the Sm core in the crystal structure of human U1 snRNP. *EMBO J.* 2010; 29:4172–4184. [PubMed: 21113136]
30. Verkoczy L, Chen Y, Zhang J, Bouton-Verville H, Newman A, Lockwood B, Scarce RM, Montefiori DC, Dennison SM, Xia S-M, Hwang K-K, Liao H-X, Alam SM, Haynes BF. Induction

of HIV-1 broad neutralizing antibodies in 2F5 knock-in mice: Selection against membrane proximal external region-associated autoreactivity limits T-dependent responses. *J. Immunol.* 2013; 191:2538–2550. [PubMed: 23918977]

31. Zhang R, Verkoczy L, Wiehe K, Munir Alam S, Nicely NI, Santra S, Bradley T, Pemble CW IV, Zhang J, Gao F, Montefiori DC, Bouton-Verville H, Kelsoe G, Larimore K, Greenberg PD, Parks R, Foulger A, Peel JN, Luo K, Lu X, Trama AM, Vandergrift N, Tomaras GD, Kepler TB, Moody MA, Liao H-X, Haynes BF. Initiation of immune tolerance-controlled HIV gp41 neutralizing B cell lineages. *Sci. Transl. Med.* 2016; 8:336ra62.
32. Liao H-X, Chen X, Munshaw S, Zhang R, Marshall DJ, Vandergrift N, Whitesides JF, Lu X, Yu J-S, Hwang K-K, Gao F, Markowitz M, Heath SL, Bar KJ, Goepfert PA, Montefiori DC, Shaw GC, Alam SM, Margolis DM, Denny TN, Boyd SD, Marshal E, Egholm M, Simen BB, Hanczaruk B, Fire AZ, Voss G, Kelsoe G, Tomaras GD, Moody MA, Kepler TB, Haynes BF. Initial antibodies binding to HIV-1 gp41 in acutely infected subjects are polyreactive and highly mutated. *J. Exp. Med.* 2011; 208:2237–2249. [PubMed: 21987658]
33. Trama AM, Moody MA, Alam SM, Jaeger FH, Lockwood B, Parks R, Lloyd KE, Stolarчук C, Scarce R, Foulger A, Marshall DJ, Whitesides JF, Jeffries TL Jr, Wiehe K, Morris L, Lambson B, Soderberg K, Hwang K-K, Tomaras GD, Vandergrift N, Jackson KJL, Roskin KM, Boyd SD, Kepler TB, Liao H-X, Haynes BF. HIV-1 envelope gp41 antibodies can originate from terminal ileum B cells that share cross-reactivity with commensal bacteria. *Cell Host Microbe.* 2014; 16:215–226. [PubMed: 25121750]
34. Williams WB, Liao H-X, Moody MA, Kepler TB, Alam SM, Gao F, Wiehe K, Trama AM, Jones K, Zhang R, Song H, Marshall DJ, Whitesides JF, Sawatzki K, Hua A, Liu P, Tay MZ, Seaton KE, Shen X, Foulger A, Lloyd KE, Parks R, Pollara J, Ferrari G, Yu J-S, Vandergrift N, Montefiori DC, Sobieszczyk ME, Hammer S, Karuna S, Gilbert P, Grove D, Grunenberger N, McElrath MJ, Mascola JR, Koup RA, Corey L, Nabel GJ, Morgan C, Churchyard G, Maenza J, Keefer M, Graham BS, Baden LR, Tomaras GD, Haynes BF. Diversion of HIV-1 vaccine-induced immunity by gp41-microbiota cross-reactive antibodies. *Science.* 2015; 349:aab1253. [PubMed: 26229114]
35. Alam SM, McAdams M, Boren D, Rak M, Scarce RM, Gao F, Camacho ZT, Gewirth D, Kelsoe G, Chen P, Haynes BF. The role of antibody polyspecificity and lipid reactivity in binding of broadly neutralizing anti-HIV-1 envelope human monoclonal antibodies 2F5 and 4E10 to glycoprotein 41 membrane proximal envelope epitopes. *J. Immunol.* 2007; 178:4424–4435. [PubMed: 17372000]
36. Alam SM, Morelli M, Dennison SM, Liao H-X, Zhang R, Xia S-M, Rits-Volloch S, Sun L, Harrison SC, Haynes BF, Chen B. Role of HIV membrane in neutralization by two broadly neutralizing antibodies. *Proc. Natl. Acad. Sci. U.S.A.* 2009; 106:20234–20239. [PubMed: 19906992]
37. Alam SM, Liao H-X, Dennison SM, Jaeger F, Parks R, Anasti K, Foulger A, Donathan M, Lucas J, Verkoczy L, Nicely N, Tomaras GD, Kelsoe G, Chen B, Kepler TB, Haynes BF. Differential reactivity of germ line allelic variants of a broadly neutralizing HIV-1 antibody to a gp41 fusion intermediate conformation. *J. Virol.* 2011; 85:11725–11731. [PubMed: 21917975]
38. Frey G, Chen J, Rits-Volloch S, Freeman MM, Zolla-Pazner S, Chen B. Distinct conformational states of HIV-1 gp41 are recognized by neutralizing and non-neutralizing antibodies. *Nat. Struct. Mol. Biol.* 2010; 17:1486–1491. [PubMed: 21076402]
39. Frey G, Peng H, Rits-Volloch S, Morelli M, Cheng Y, Chen B. A fusion-intermediate state of HIV-1 gp41 targeted by broadly neutralizing antibodies. *Proc. Natl. Acad. Sci. U.S.A.* 2008; 105:3739–3744. [PubMed: 18322015]
40. Shen X, Dennison SM, Liu P, Gao F, Jaeger F, Montefiori DC, Verkoczy L, Haynes BF, Alam SM, Tomaras GD. Prolonged exposure of the HIV-1 gp41 membrane proximal region with L669S substitution. *Proc. Natl. Acad. Sci. U.S.A.* 2010; 107:5972–5977. [PubMed: 20231447]
41. Lavinder JJ, Horton AP, Georgiou G, Ippolito GC. Next-generation sequencing and protein mass spectrometry for the comprehensive analysis of human cellular and serum antibody repertoires. *Curr. Opin. Chem. Biol.* 2015; 24:112–120. [PubMed: 25461729]
42. Wrammert J, Koutsonanos D, Li G-M, Edupuganti S, Sui J, Morrissey M, McCausland M, Skountzou I, Hornig M, Lipkin WI, Mehta A, Razavi B, Del Rio C, Zheng N-Y, Lee J-H, Huang M, Ali Z, Kaur K, Andrews S, Amara RR, Wang Y, Das SR, O'Donnell CD, Yewdell JW,

- Subbarao K, Marasco WA, Mulligan MJ, Compans R, Ahmed R, Wilson PC. Broadly cross-reactive antibodies dominate the human B cell response against 2009 pandemic H1N1 influenza virus infection. *J. Exp. Med.* 2011; 208:181–193. [PubMed: 21220454]
43. Purtha WE, Tedder TF, Johnson S, Bhattacharya D, Diamond MS. Memory B cells, but not long-lived plasma cells, possess antigen specificities for viral escape mutants. *J. Exp. Med.* 2011; 208:2599–2606. [PubMed: 22162833]
44. Levesque MC, Moody MA, Hwang K-K, Marshall DJ, Whitesides JF, Amos JD, Gurley TC, Allgood S, Haynes BB, Vandergrift NA, Plonk S, Parker DC, Cohen MS, Tomaras GD, Goepfert PA, Shaw GM, Schmitz JE, Eron JJ, Shaheen NJ, Hicks CB, Liao H-X, Markowitz M, Kelsoe G, Margolis DM, Haynes BF. Polyclonal B cell differentiation and loss of gastrointestinal tract germinal centers in the earliest stages of HIV-1 infection. *PLOS Med.* 2009; 6:e1000107. [PubMed: 19582166]
45. Moir S, Ho J, Malaspina A, Wang W, DiPoto AC, O’Shea MA, Roby G, Kottlilil S, Arthos J, Proschan MA, Chun T-W, Fauci AS. Evidence for HIV-associated B cell exhaustion in a dysfunctional memory B cell compartment in HIV-infected viremic individuals. *J. Exp. Med.* 2008; 205:1797–1805. [PubMed: 18625747]
46. Irimia A, Sarkar A, Stanfield RL, Wilson IA. Crystallographic identification of lipid as an integral component of the epitope of HIV broadly neutralizing antibody 4E10. *Immunity.* 2016; 44:21–31. [PubMed: 26777395]
47. Lee JH, Ozorowski G, Ward AB. Cryo-EM structure of a native, fully glycosylated, cleaved HIV-1 envelope trimer. *Science.* 2016; 351:1043–1048. [PubMed: 26941313]
48. Yang G, Holl TM, Liu Y, Li Y, Lu X, Nicely NI, Kepler TB, Alam SM, Liao H-X, Cain DW, Spicer L, VandeBerg JL, Haynes BF, Kelsoe G. Identification of autoantigens recognized by the 2F5 and 4E10 broadly neutralizing HIV-1 antibodies. *J. Exp. Med.* 2013; 210:241–256. [PubMed: 23359068]
49. Moody MA, Pedroza-Pacheco I, Vandergrift NA, Chui C, Lloyd KE, Parks R, Soderberg KA, Ogbe AT, Cohen MS, Liao H-X, Gao F, McMichael AJ, Montefiori DC, Verkoczy L, Kelsoe G, Huang J, Shea PR, Connors M, Borrow P, Haynes BF. Immune perturbations in HIV-1-infected individuals who make broadly reactive neutralizing antibodies. *Sci. Immunol.* 2016; 1:aag0851. [PubMed: 28783677]
50. Hraber P, Seaman MS, Bailer RT, Mascola JR, Montefiori DC, Korber BT. Prevalence of broadly neutralizing antibody responses during chronic HIV-1 infection. *AIDS.* 2014; 28:163–169. [PubMed: 24361678]
51. Tomaras GD, Binley JM, Gray ES, Crooks ET, Osawa K, Moore PL, Tumba N, Tong T, Shen X, Yates NL, Decker J, Wibmer CK, Gao F, Alam SM, Easterbrook P, Abdool Karim S, Kamanga G, Crump JA, Cohen M, Shaw GM, Mascola JR, Haynes BF, Montefiori DC, Morris L. Polyclonal B cell responses to conserved neutralization epitopes in a subset of HIV-1-infected individuals. *J. Virol.* 2011; 85:11502–11519. [PubMed: 21849452]
52. Chuang G-Y, Acharya P, Schmidt SD, Yang Y, Louder MK, Zhou T, Kwon YD, Pancera M, Bailer RT, Doria-Rose NA, Nussenzweig MC, Mascola JR, Kwong PD, Georgiev IS. Residue-level prediction of HIV-1 antibody epitopes based on neutralization of diverse viral strains. *J. Virol.* 2013; 87:10047–10058. [PubMed: 23843642]
53. Gray ES, Taylor N, Wycuff D, Moore PL, Tomaras GD, Wibmer CK, Puren A, DeCamp A, Gilbert PB, Wood B, Montefiori DC, Binley JM, Shaw GM, Haynes BF, Mascola JR, Morris L. Antibody specificities associated with neutralization breadth in plasma from human immunodeficiency virus type 1 subtype C-infected blood donors. *J. Virol.* 2009; 83:8925–8937. [PubMed: 19553335]
54. Tiller T, Meffre E, Yurasov S, Tsuiji M, Nussenzweig MC, Wardemann H. Efficient generation of monoclonal antibodies from single human B cells by single cell RT-PCR and expression vector cloning. *J. Immunol. Methods.* 2008; 329:112–124. [PubMed: 17996249]
55. Liao H-X, Levesque MC, Nagel A, Dixon A, Zhang R, Walter E, Parks R, Whitesides J, Marshall DJ, Hwang K-K, Yang Y, Chen X, Gao F, Munshaw S, Kepler TB, Denny T, Moody MA, Haynes BF. High-throughput isolation of immunoglobulin genes from single human B cells and expression as monoclonal antibodies. *J. Virol. Methods.* 2009; 158:171–179. [PubMed: 19428587]
56. Kepler TB. Reconstructing a B-cell clonal lineage. I. Statistical inference of unobserved ancestors. *F1000Res.* 2013; 2:103. [PubMed: 24555054]

57. Liao H-X, Lynch R, Zhou T, Gao F, Alam SM, Boyd SD, Fire AZ, Roskin KM, Schramm CA, Zhang Z, Zhu J, Shapiro L, NISC Comparative Sequencing Program, Mullikin JC, Gnanakaran S, Hraber P, Wiehe K, Kelsoe G, Yang G, Xia S-M, Montefiori DC, Parks R, Lloyd KE, Searce RM, Soderberg KA, Cohen M, Kamanga G, Louder MK, Tran LM, Chen Y, Cai F, Chen S, Moquin S, Du X, Joyce MG, Srivatsan S, Zhang B, Zheng A, Shaw GM, Hahn BH, Kepler TB, Korber BTM, Kwong PD, Mascola JR, Haynes BF. Co-evolution of a broadly neutralizing HIV-1 antibody and founder virus. *Nature*. 2013; 496:469–476. [PubMed: 23552890]
58. Gao F, Bonsignori M, Liao H-X, Kumar A, Xia S-M, Lu X, Cai F, Hwang K-K, Song H, Zhou T, Lynch RM, Alam SM, Moody MA, Ferrari G, Berrong M, Kelsoe G, Shaw GM, Hahn BH, Montefiori DC, Kamanga G, Cohen MS, Hraber P, Kwong PD, Korber BT, Mascola JR, Kepler TB, Haynes BF. Cooperation of B cell lineages in induction of HIV-1-broadly neutralizing antibodies. *Cell*. 2014; 158:481–491. [PubMed: 25065977]
59. Kepler TB, Munshaw S, Wiehe K, Zhang R, Yu J-S, Woods CW, Denny TN, Tomaras GD, Alam SM, Moody MA, Kelsoe G, Liao H-X, Haynes BF. Reconstructing a B-cell clonal lineage. II. Mutation, selection, and affinity maturation. *Front. Immunol.* 2014; 5:170. [PubMed: 24795717]
60. Felstein, J. PHYLIP (Phylogeny Inference Package) Version 3.69. Department of Genome Sciences, University of Washington; 2009.
61. Bolotin DA, Poslavsky S, Mitrophanov I, Shugay M, Mamedov IZ, Putintseva EV, Chudakov DM. MiXCR: Software for comprehensive adaptive immunity profiling. *Nat. Methods*. 2015; 12:380–381. [PubMed: 25924071]
62. Magoč T, Salzberg SL. FLASH: Fast length adjustment of short reads to improve genome assemblies. *Bioinformatics*. 2011; 27:2957–2963. [PubMed: 21903629]
63. Alamyar E, Duroux P, Lefranc M-P, Giudicelli V. IMGT® tools for the nucleotide analysis of immunoglobulin (IG) and T cell receptor (TR) V-(D)-J repertoires, polymorphisms, and IG mutations: IMGT/V-QUEST and IMGT/HighV-QUEST for NGS. *Methods Mol. Biol.* 2012; 882:569–604. [PubMed: 22665256]
64. Wine Y, Boutz DR, Lavinder JJ, Miklos AE, Hughes RA, Hoi KH, Jung ST, Horton AP, Murrin EM, Ellington AD, Marcotte EM, Georgiou G. Molecular deconvolution of the monoclonal antibodies that comprise the polyclonal serum response. *Proc. Natl. Acad. Sci. U.S.A.* 2013; 110:2993–2998. [PubMed: 23382245]
65. Montefiori, DC. *Current Protocols in Immunology*. John Wiley & Sons; 2005. Evaluating neutralizing antibodies against HIV, SIV, and SHIV in luciferase reporter gene assays. chap. 12
66. Seaman MS, Janes H, Hawkins N, Grandpre LE, Devoy C, Giri A, Coffey RT, Harris L, Wood B, Daniels MG, Bhattacharya T, Lapedes A, Polonis VR, McCutchan FE, Gilbert PB, Self SG, Korber BT, Montefiori DC, Mascola JR. Tiered categorization of a diverse panel of HIV-1 Env pseudoviruses for assessment of neutralizing antibodies. *J. Virol.* 2010; 84:1439–1452. [PubMed: 19939925]
67. Nielsen M, Lundegaard C, Lund O, Petersen TN. CPHmodels-3.0-remote homology modeling using structure-guided sequence profiles. *Nucleic Acids Res.* 2010; 38:W576–W581. [PubMed: 20542909]
68. Humphrey W, Dalke A, Schulten K. VMD: Visual molecular dynamics. *J. Mol. Graph.* 1996; 14:33–38. [PubMed: 8744570]
69. Alam SM, Liao H-X, Tomaras GD, Bonsignori M, Tsao C-Y, Hwang K-K, Chen H, Lloyd KE, Bowman C, Sutherland L, Jeffries TL Jr, Kozink DM, Stewart S, Anasti K, Jaeger FH, Parks R, Yates NL, Overman RG, Sinangil F, Berman PW, Pitisuttithum P, Kaewkungwal J, Nitayaphan S, Karasavva N, Rerks-Ngarm S, Kim JH, Michael NL, Zolla-Pazner S, Santra S, Letvin NL, Harrison SC, Haynes BF. Antigenicity and immunogenicity of RV144 vaccine AIDSVAX clade E envelope immunogen is enhanced by a gp120 N-terminal deletion. *J. Virol.* 2013; 87:1554–1568. [PubMed: 23175357]
70. Haynes BF, Fleming J, St Clair EW, Katinger H, Stiegler G, Kunert R, Robinson J, Searce RM, Plonk K, Staats HF, Ortel TL, Liao H-X, Alam SM. Cardiolipin polyspecific autoreactivity in two broadly neutralizing HIV-1 antibodies. *Science*. 2005; 308:1906–1908. [PubMed: 15860590]
71. Liu P, Yates NL, Shen X, Bonsignori M, Moody MA, Liao H-X, Fong Y, Alam SM, Overman RG, Denny T, Ferrari G, Ochsenbauer C, Kappes JC, Polonis VR, Pitisuttithum P, Kaewkungwal J, Nitayaphan S, Rerks-Ngarm S, Montefiori DC, Gilbert P, Michael NL, Kim JH, Haynes BF,

- Tomaras GD. Infectious virion capture by HIV-1 gp120-specific IgG from RV144 vaccinees. *J. Virol.* 2013; 87:7828–7836. [PubMed: 23658446]
72. Liu P, Williams LD, Shen X, Bonsignori M, Vandergrift NA, Overman RG, Moody MA, Liao H-X, Stieh DJ, McCotter KL, French AL, Hope TJ, Shattock R, Haynes BF, Tomaras GD. Capacity for infectious HIV-1 virion capture differs by envelope antibody specificity. *J. Virol.* 2014; 88:5165–5170. [PubMed: 24554654]
73. Sun Z-YJ, Oh KJ, Kim M, Yu J, Brusica V, Song L, Qiao Z, Wang J-h, Wagner G, Reinherz EL. HIV-1 broadly neutralizing antibody extracts its epitope from a kinked gp41 ectodomain region on the viral membrane. *Immunity.* 2008; 28:52–63. [PubMed: 18191596]
74. Adams PD, Afonine PV, Bunkóczi G, Chen VB, Davis IW, Echols N, Headd JJ, Hung L-W, Kapral GJ, Grosse-Kunstleve RW, McCoy AJ, Moriarty NW, Oeffner R, Read RJ, Richardson DC, Richardson JS, Terwilliger TC, Zwart PH. PHENIX: A comprehensive Python-based system for macromolecular structure solution. *Acta Crystallogr. Sect. D.* 2010; D66:213–221.
75. Burke V, Williams C, Sukumaran M, Kim S-S, Li H, Wang X-H, Gorny MK, Zolla-Pazner S, Kong X-P. Structural basis of the cross-reactivity of genetically related human anti-HIV-1 mAbs: Implications for design of V3-based immunogens. *Structure.* 2009; 17:1538–1546. [PubMed: 19913488]
76. Teplyakov A, Luo J, Obmolova G, Malia TJ, Sweet R, Stanfield RL, Kodangattil S, Almagro JC, Gilliland GL. Antibody modeling assessment II. Structures and models. *Proteins.* 2014; 82:1563–1582. [PubMed: 24633955]
77. Adams PD, Grosse-Kunstleve RW, Hung L-W, Ioerger TR, McCoy AJ, Moriarty NW, Read RJ, Sacchettini JC, Sauter NK, Terwilliger TC. PHENIX: Building new software for automated crystallographic structure determination. *Acta Crystallogr. Sect. D.* 2002; D58:1948–1954.
78. Emsley P, Cowtan K. Coot: Model-building tools for molecular graphics. *Acta Crystallogr. Sect. D.* 2004; D60:2126–2132.
79. Krissinel E, Henrick K. Inference of macromolecular assemblies from crystalline state. *J. Mol. Biol.* 2007; 372:774–797. [PubMed: 17681537]
80. Winn MD, Ballard CC, Cowtan KD, Dodson EJ, Emsley P, Evans PR, Keegan RM, Krissinel EB, Leslie AGW, McCoy A, McNicholas SJ, Murshudov GN, Pannu NS, Pottertone EA, Powell HR, Read RJ, Vagin A, Wilson KS. Overview of the CCP4 suite and current developments. *Acta Crystallogr. Sect. D.* 2011; D67:235–242.

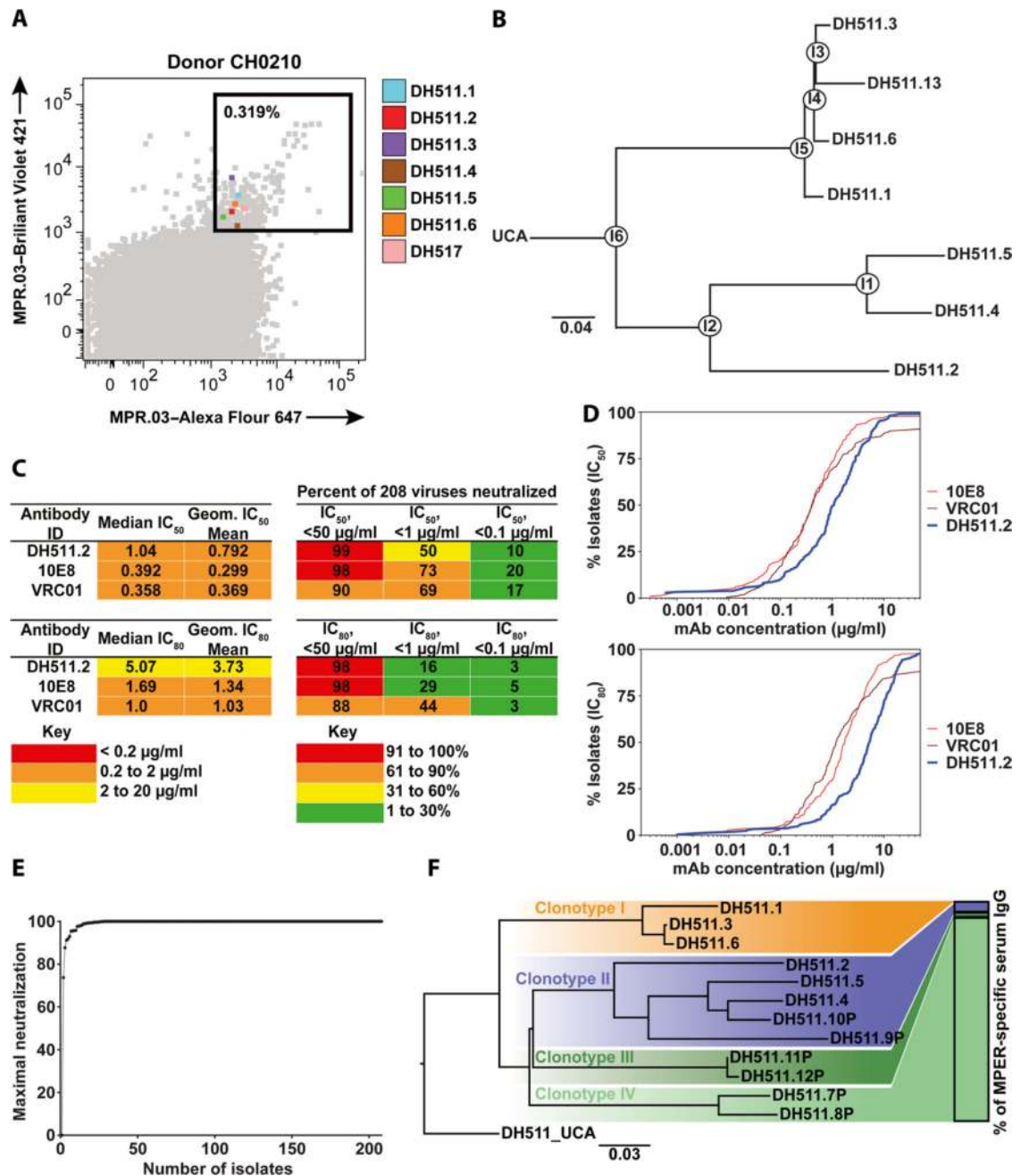


Fig. 1. Isolation of MPER-directed bnAbs

(A) Fluorescently labeled MPR.03 peptide tetramers were used to decorate PBMCs from donor CH0210. A flow cytometric plot is shown. The square represents frequency of MPR.03 double-positive MPER-specific memory B cells that were sorted for Ig gene amplification and expression. Colored dots within the square show individual cells that yielded MPER-specific mAbs DH511.1 to DH511.6 and DH517, as revealed by index sorting. Memory B cells were gated as live CD16⁻CD14⁻CD3⁻CD235⁻CD19⁺IgD⁻/CD38^{all}. (B) Phylogenetic tree of V_HD_HJ_H sequences of the DH511 clonal lineage. Ancestral reconstruction of the evolutionary pathway from the inferred UCA to the mature

mAbs including six maturational intermediates (I1 to I6, circles). DH511.13 could not be expressed and was not studied further. (C) Neutralization activity of probe-identified MPER antibodies against a panel of 208 cross-clade HIV-1 isolates. Median and geometric mean neutralization potency against viruses neutralized with an IC_{50}/IC_{80} of $<50 \mu\text{g/ml}$. Right: The percentage of 208 viruses neutralized by mAbs DH511.2, 10E8, and VRC01 at IC_{50} or IC_{80} of $<50 \mu\text{g/ml}$, $<1 \mu\text{g/ml}$, and $<0.1 \mu\text{g/ml}$. (D) Neutralization potency and breadth of DH511.2 compared with 10E8 and VRC01 against a 208-isolate HIV-1 Env pseudovirus panel displayed as potency-breadth curves. The percentage of isolates neutralized at IC_{50} (top) and IC_{80} (bottom) values is plotted against mAb concentration. (E) Percent maximum neutralization of each isolate by DH511.2. (F) Identification of MPER-directed broadly neutralizing plasma antibodies by proteomics. Phylogenetic tree of heavy chain sequences identified in the plasma and added to DH511.1 to DH511.6 isolated from the memory B cell compartment [see (B)]. The bar on the right shows the relative abundance of the three identified clonotypes in serum (IV, 95%; II, 4%; III, 1%).

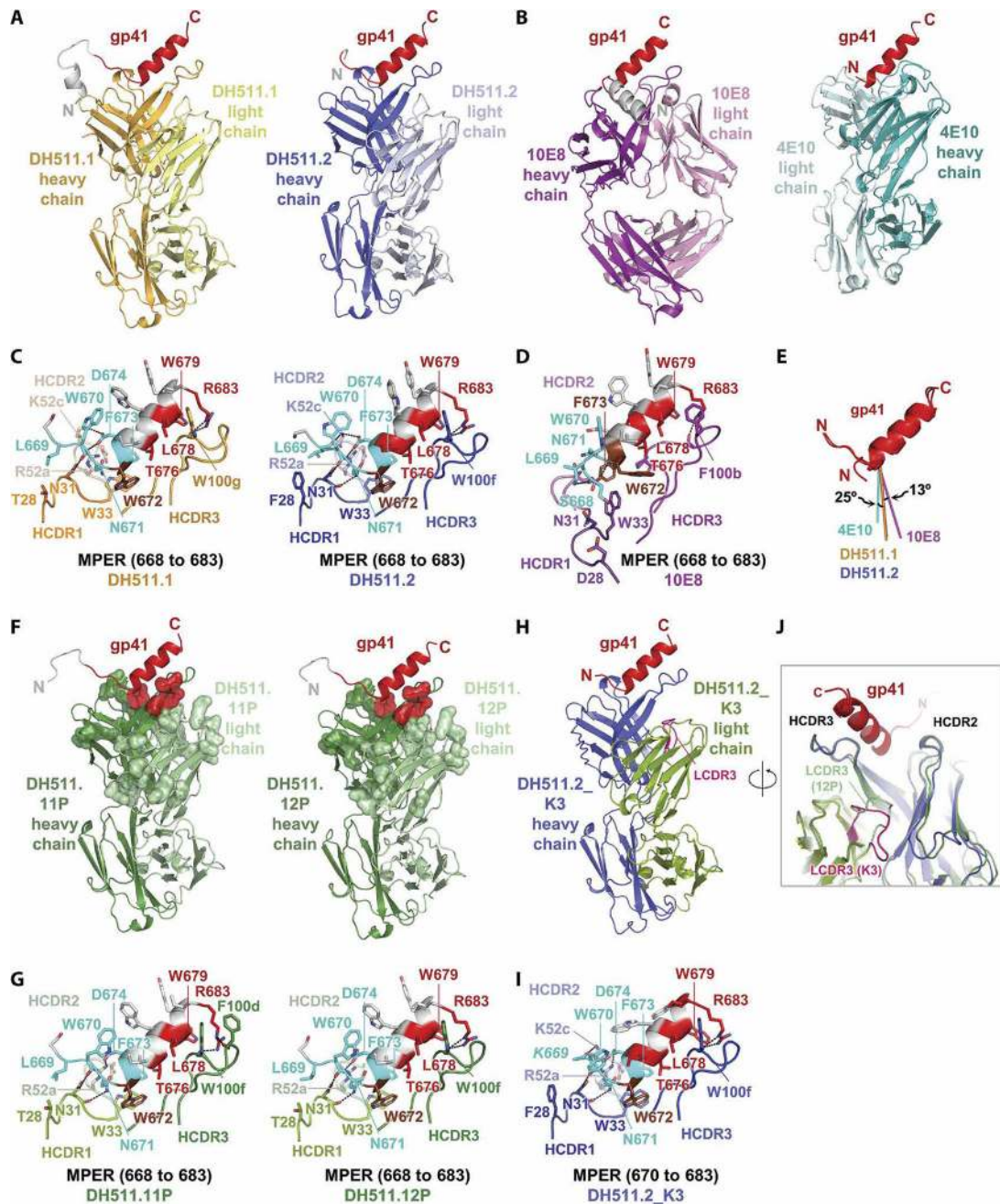


Fig. 2. Structural analysis of the DH511 lineage

(A) Crystal structures of DH511.1 and DH511.2 Fabs in complex with gp41 MPER peptides 656 to 683 and 662 to 683, respectively, oriented on the basis of C α atom superposition of distal MPER residues. MPER residues 668 to 683 are colored red. (B) Crystal structures of antibodies 10E8 (PDB: 4G6F) and 4E10 (PDB: 2FX7) in complex with MPER, oriented as in (A). Close-up view of DH511.1 and DH511.2 (C) and 10E8 (D) contacts with MPER residues 668 to 683. MPER residues that interact with antibody V_H3–15 region residues, HCDR3 residues, or both are shown in cyan, red, or brown, respectively. (E) Directions of approach to distal gp41 MPER by antibodies DH511.1, DH511.2, 10E8, and 4E10. Shown

are superimposed structures of antibody-bound gp41 MPER, with lines representing antibody variable region directions of approach colored as in (A) and (B). **(F)** Crystal structures of Fabs of plasma-derived variants DH511.11P and DH511.12P in complex with gp41 MPER peptide 662 to 683, with residues 668 to 683 colored red. Antibody residues shown in surface representation differ in sequence from DH511.1 or DH511.2, with those at the interface with gp41 shown in red. **(G)** Close-up view of DH511.11P and DH511.12P contacts with MPER residues 668 to 683, colored as in (C). **(H)** Crystal structure of chimeric antibody DH511.2_K3 in complex with MPER peptide 670 to 683, with a close-up view shown in **(I)** and colored as in (C). **(J)** Close-up view of the LCDR3 loop of DH511.2.K3 (magenta), rotated along the antibody longitudinal axis relative to (H) and superimposed with the complex structure of DH511.12P.

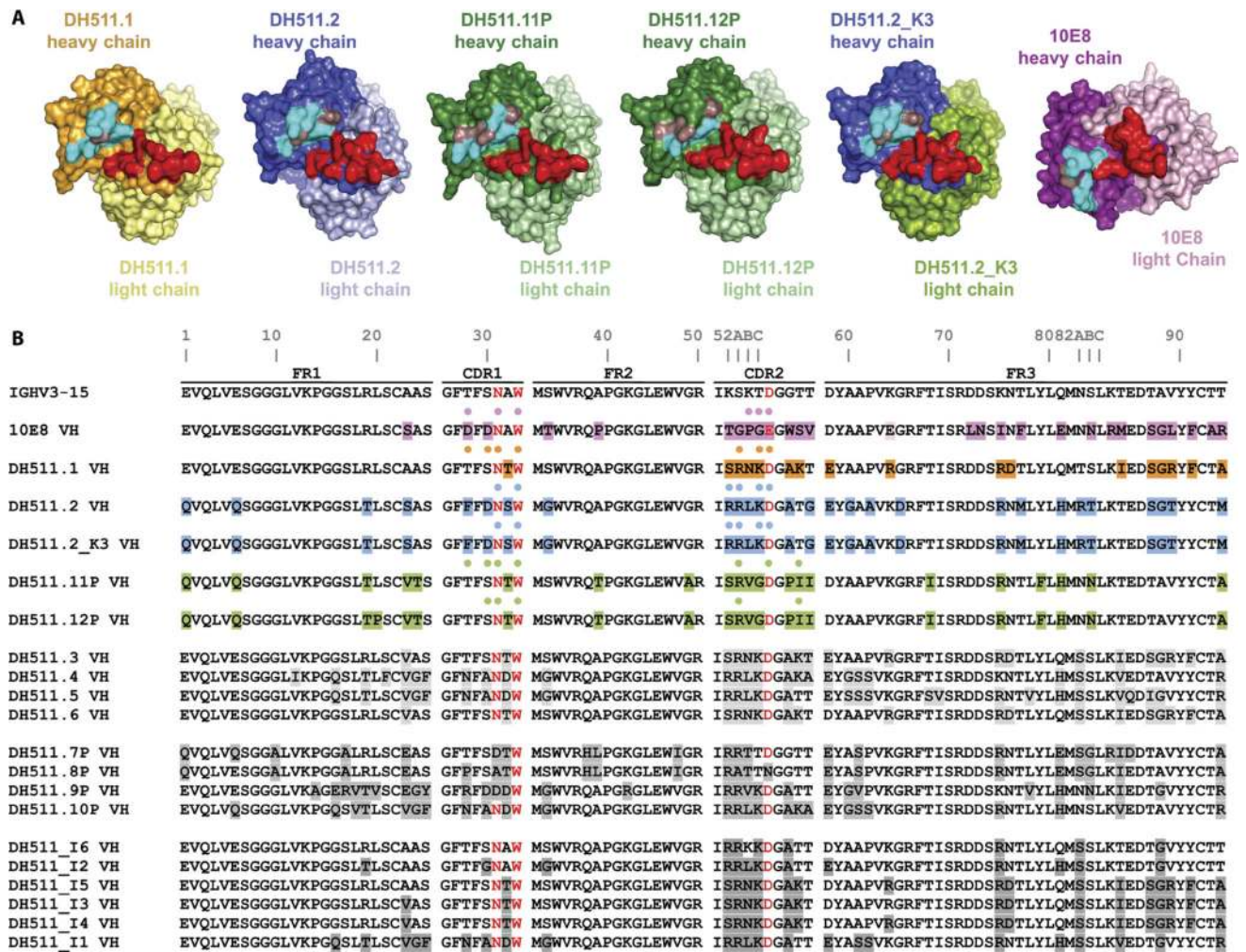


Fig. 3. Comparison of paratopes of DH511 lineage antibodies with 10E8 MPER bnAb
(A) Surface representations of DH511 lineage antibodies and 10E8, rotated by 60° toward the reader, relative to the orientations in Fig.2. Antibody residues at positions within the heavy chain V_H3-15 region that mediate contacts with gp41 in both the DH511 and 10E8 lineages are shown in cyan. Remaining gp41-contacting residues within the V_H3-15 region of the respective antibodies are shown in dark violet. HCDR3 residues that contact gp41 are shown in red. **(B)** Sequence alignment of DH511 lineage antibodies from memory B cells, plasma, and inferred intermediates, against antibody 10E8 and their shared V_H3-15 germline gene precursor. Residues that contact gp41 in the crystal structures are labeled with closed circles; somatically mutated residues are shaded. Conserved V_H3-15 germline residues that interact with gp41 are shown in red.

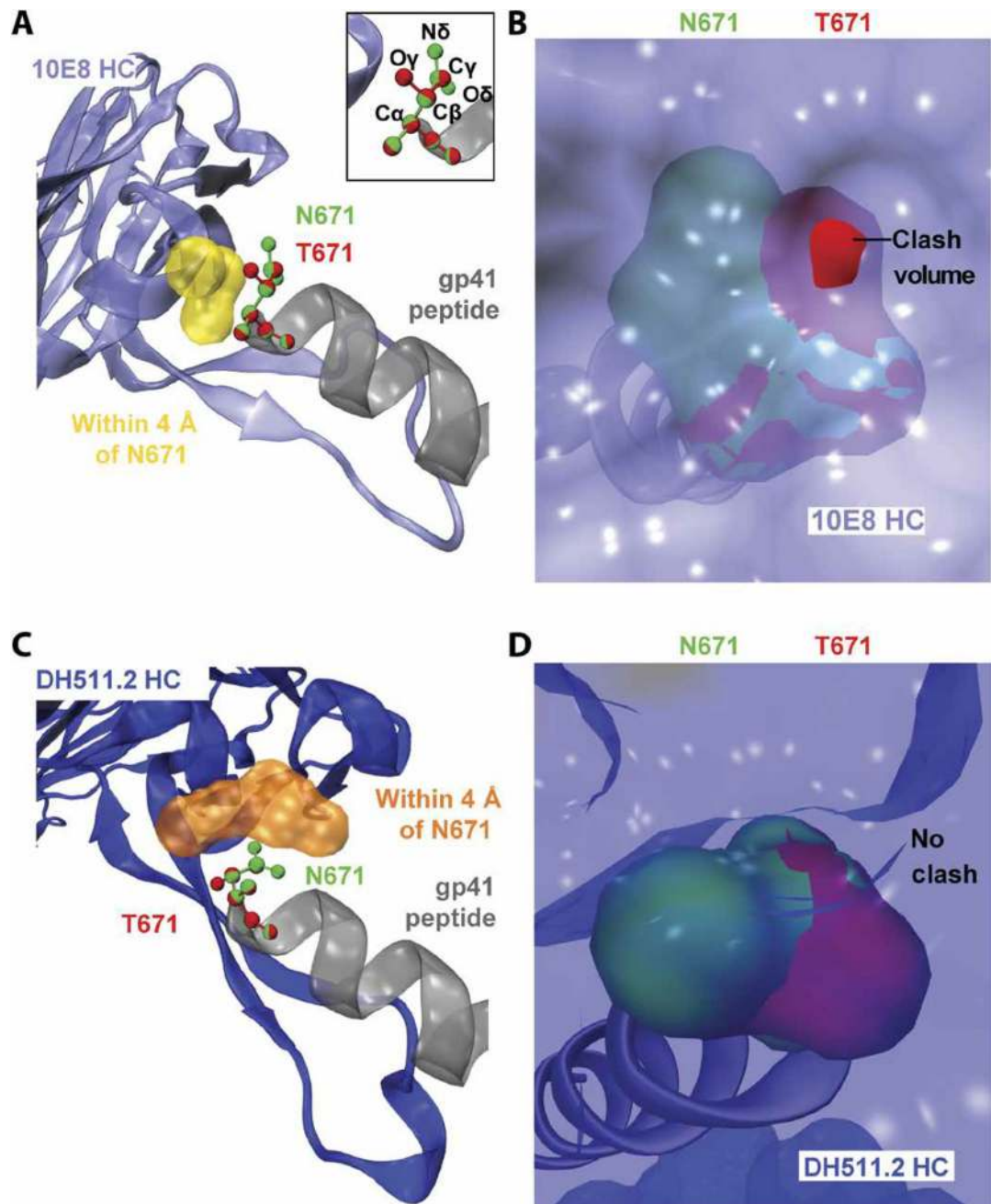


Fig. 4. Interactions of HIV-1 Env gp41 Asn and Thr at position 671 with distal MPER bnAbs 10E8 and DH511.2

(A) 10E8 heavy chain (lavender) is shown in complex with gp41 MPER peptide (gray), with Asn (green, original amino acid in the structure) and Thr (red, modeled) at 671 shown in ball and stick representations. The 10E8 heavy chain volume within 4 Å of Asn⁶⁷¹ is shown in yellow surface representation. Inset: Alignment of the modeled side chain for Thr with the Asn from the crystal structure, with various heavy atoms labeled. The crystal structure from PDB 4G6F (1) was used. (B) View of Asn (green opaque) and Thr⁶⁷¹ (red opaque) surfaces from within the 10E8 heavy chain (HC) surface (lavender transparent). A part of the Thr⁶⁷¹ surface penetrates the 10E8 heavy chain clash volume. A cutoff of 1.4 Å around each heavy

atom was used to render the amino acid surfaces. (C) Same as in (A) with DH511.2 heavy chain shown in blue and with DH511.2 heavy chain volume within 4 Å of Asn⁶⁷¹ shown in orange. gp41 peptide is aligned such that Env positions 673 to 685 have the same arrangement as in (A). The relative position of Thr compared with Asn was very similar, as shown in the inset of (A). (D) Same as in (B), with DH511.2 heavy chain volume shown as transparent blue. No part of the Thr⁶⁷¹ amino acid surface penetrated the DH511.2 volume.

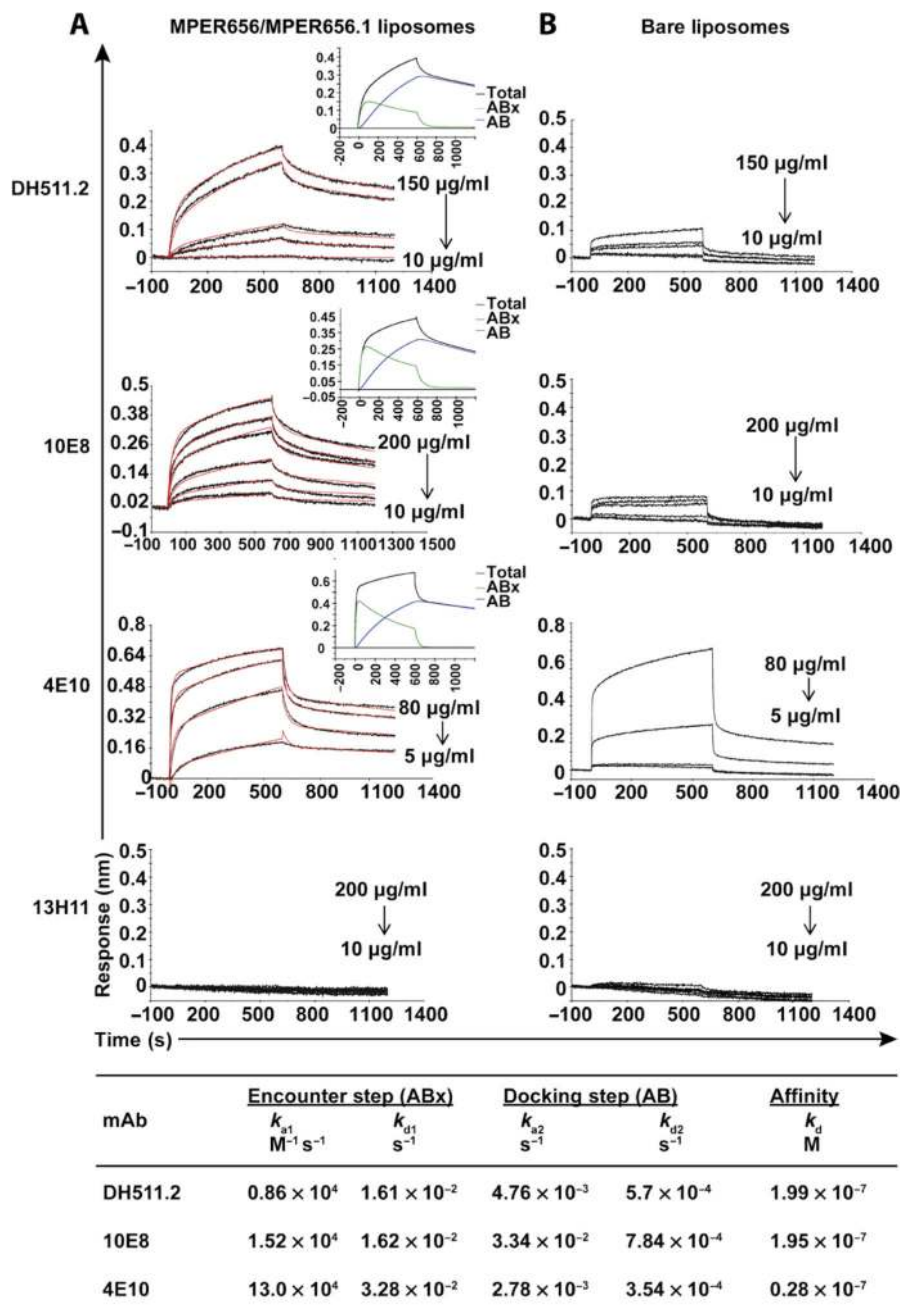


Fig. 5. Comparison of DH511.2 binding to MPER peptide liposome conjugates to that of distal MPER bnAbs 4E10 and 10E8

(A) Both DH511.2 and 10E8 mAb binding to MPER liposomes followed a two-step “encounter-docking” model [$A + B \rightarrow ABx$ (encounter step); $ABx \rightarrow AB$ (docking step)] and was similar to the mode of binding of the MPER bnAb 4E10. The experimental data for each concentration of the indicated mAbs are shown in black, and the fitted curves derived from global curve fitting to the two-step conformational model are shown in red. Decreasing concentration dose of each mAb is as follows: DH511.2 = 1000, 666.7, 333.3, 166.7, and 66.7 nM; 10E8 = 1333.3, 1000, 666.7, 333.3, 166.7, and 66.7 nM; 4E10 = 533.3, 266.7, 66.7, and 33.3 nM; 13H11 = 2000, 1000, 666.7, 533.3, 333.3, 266.7, 133.3, and 66.7 nM.

The inset for each of the indicated MPER bnAbs shows the component curves for the encounter (Abx; green) and docked (AB; blue) complexes. The calculated rate constants for each binding step are shown in the table at the bottom. **(B)** Raw (control unsubtracted) binding of each mAb to bare (peptide-free) liposomes of the same lipid composition as the MPER liposomes. The control and non-neutralizing MPER 13H11 mAb show no binding to either MPER liposomes or bare (peptide-free) liposomes. MPER656 or MPER656.1 peptide was conjugated to synthetic liposomes for binding to 10E8 or DH511.2, respectively, and binding analysis was performed by biolayer interferometry analysis as described in the Materials and Methods. Data are representative of two independent experiments.

Author Manuscript

Author Manuscript

Author Manuscript

Author Manuscript

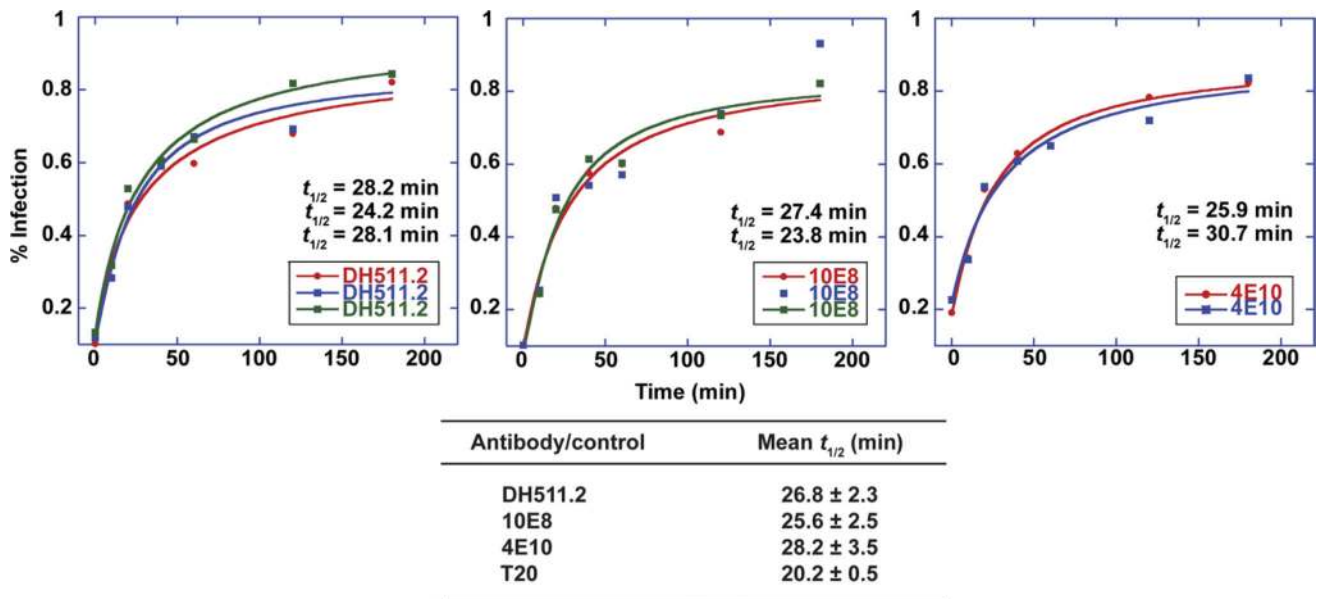


Fig. 6. DH511.2 recognizes a transiently exposed intermediate state of gp41, and the lifetime of DH511.2 epitope exposure is the same as that of 10E8 and 4E10

Time course of neutralization of the tier 2 HIV-1 isolate B.BG1168 was measured by addition of mAbs to TZM-bl cells preincubated with virus. The mean $t_{1/2}$ half-life of neutralization \pm SD values were derived from four-parametric sigmoid curve fitting analysis using data from two or three independent experiments. Half-life values were similar among the three antibodies.